Simulating the Global Distribution of Nitrogen Isotopes in the Ocean

Christopher Somes, Andreas Schmittner, Alan Mix, Ricardo Letelier
College of Oceanic and Atmospheric Sciences, Oregon State University, Corvallis, Oregon, USA

Eric Galbraith
Department of Earth and Planetary Science, McGill University, Montreal, Quebec, Canada

Moritz F. Lehmann
Institute for Environmental Geoscience, Basel University, Basel, Switzerland

Mark Altabet
School for Marine Science and Technology, U. Massachusetts Dartmouth, New Bedford, Massachusetts, USA

Joseph Montoya
School of Biology, Georgia Institute of Technology, Atlanta, Georgia, USA

Michael Eby, Annie Bourbonnais
School of Earth and Ocean Sciences, University of Victoria, Victoria, British Columbia, Canada

Abstract

We present a new nitrogen isotope model incorporated into the three-dimensional ocean component of a global Earth System Climate Model designed for millennial timescale simulations. The model includes prognostic tracers for the two stable nitrogen isotopes, ^{14}N and ^{15}N, in the nitrate (NO_3^-), phytoplankton, zooplankton, and detritus variables of the marine ecosystem model. The isotope effects of algal NO_3^- uptake, nitrogen fixation, water column denitrification, and zooplankton excretion are considered as well as the removal of NO_3^- by sedimentary denitrification. A global database of $\delta^{15}NO_3^-$ observations is compiled from previous studies and compared to the model results on a regional basis where sufficient observations exist. The model is able to qualitatively and quantitatively reproduce many of the observed patterns such as high subsurface values in water column denitrification zones and the meridional and vertical gradients in the Southern Ocean. The observed pronounced subsurface minimum in the Atlantic is underestimated by the model presumably owing to too little simulated nitrogen fixation there. Sensitivity experiments reveal that algal NO_3^- uptake, nitrogen

fixation and water column denitrification have the strongest effects on the simulated distribution of nitrogen isotopes, whereas the effect from zooplankton excretion is weaker. Both water column and sedimentary denitrification also have important indirect effects on the nitrogen isotope distribution by lowering the fixed nitrogen inventory, which creates an ecological niche for nitrogen fixers and, thus, stimulates additional N_2 fixation in the model. Important model deficiencies are identified, and strategies for future improvement and possibilities for model application are outlined.

1. Introduction

Bioavailable nitrogen (fixed-N) is one of the major limiting nutrients for algal photosynthesis, which drives the sequestration of CO_2 from the surface ocean and atmosphere into the deep ocean via the sinking of organic matter. Changes in this so-called 'biological pump' have been hypothesized to account for a significant amount of the glacial-interglacial fluctuations in atmospheric CO_2 [*McElroy,* 1982; *Falkowski*, 1997]. However, the relative contributions of the biological and physical carbon pumps to CO_2 variations remain controversial. The size of the oceanic fixed-N inventory, which regulates the strength of the biological pump, is controlled by different biogeochemical processes that are difficult to constrain quantitatively in a global budget [*Codispoti*, 2007]. Nitrogen isotopes (both in dissolved and organic N species) in the water column and sea floor sediments are sensitive indicators of those processes [*Brandes and Devol*, 2002; *Altabet*, 2007].

Many N-transformational processes alter the ratio of the two stable forms of the nitrogen isotopes, ^{14}N and ^{15}N, differently, a process referred to as fractionation. Resulting variations in N isotopic composition can be described as deviations in $^{15}N/^{14}N$ ratio from an accepted standard

$$\delta^{15}N = [(^{15}N/^{14}N) / R_{std} - 1] \times 1000 \quad , \qquad (1)$$

where R_{std} is the $^{15}N/^{14}N$ ratio of atmospheric N_2 gas. Isotope fractionation can occur due to kinetic processes (i.e., different reaction rates for isotopes in a reactant-product stream). It generally results in the enrichment of the heavier ^{15}N isotope in the reaction substrate, and its depletion in the product. For example, preferential discrimination against ^{15}N relative to ^{14}N during algal NO_3^- assimilation results in net enrichment of ^{15}N in the residual NO_3^- and net depletion of ^{15}N in organic matter (OM). The degree of isotopic discrimination, or fractionation, for each process can be quantified with an enrichment factor, $\varepsilon = (^{14}k/^{15}k - 1) \bullet 1000$, where k is the specific reaction rate for each isotope [*Mariotti et al.*, 1981].

The predominant source and sink terms of the oceanic fixed-N inventory, N_2 fixation and denitrification, respectively, have their own distinct effects on the marine N isotope budgets. N_2-fixing bacteria (diazotrophs) introduce bioavailable N into the ocean close to that of atmospheric N_2 ($\delta^{15}N \approx -2 – 0‰$) [*Delwiche and Steyn*, 1970 ; *Minagawa and Wada*, 1986; *Macko et al*, 1987; *Carpenter et al.*, 1997; *Montoya et al.*, 2002]. Denitrification occurs under suboxic conditions ($O_2 < 5$ μmol/kg) in the water column and in the sea floor sediments. Here, microbes use NO_3^- instead of O_2 as the electron acceptor during respiration and convert it to gaseous forms of N (N_2O and N_2), which can then escape to the atmosphere [*Codispoti and Richards*, 1976]. The volume and distribution of suboxic water is affected by the temperature-dependent solubility of O_2 at the surface and the rate of subduction of oxygen-saturated water masses to greater depths, as well as the amount of organic matter that remineralizes in the ocean interior, both of which are sensitive to changes in climate.

Denitrifiers preferentially consume $^{14}NO_3^-$ leaving the residual oceanic NO_3^- pool strongly enriched in the heavier ^{15}N, with N isotope enrichment factors between 20 – 30‰ [*Cline and Kaplan*, 1975; *Liu*

and Kaplan, 1989; *Brandes et al*, 1998; *Altabet et al.*, 1999; *Voss et al.*, 2001; *Sigman et al.*, 2003]. Sedimentary denitrification is generally limited by the amount of NO_3^- that diffuses into the reactive zones within the sediments. Therefore, it consumes nearly all of the influxing NO_3^- available, leaving nearly unaltered $\delta^{15}N$ values in the overlying waters [*Brandes and Devol*, 1997, 2002; *Sigman et al.*, 2003; *Lehmann et al*., 2004, 2007]. The average oceanic $\delta^{15}NO_3^-$ value near 5‰ [*Sigman et al.*, 1997, 1999] can be interpreted as the balance between the isotope effects of water column denitrification, sedimentary denitrification, and N_2 fixation [*Brandes and Devol*, 2002; *Deutsch et al.*, 2004; *Galbraith et al.*, 2004; *Altabet*, 2007].

The $\delta^{15}N$ signal in the water column and sea floor sediments is also affected by fractionation processes within the food chain. Marine algae preferentially assimilate the lighter ^{14}N into their biomass with a range of enrichment factors estimated in the field between 4 – 15‰ [*Wada*, 1980; *Altabet et al.*, 1991; *Altabet and Fracois*, 1994; *Altabet et al.*, 1999; *Sigman et al.*, 1999; *Altabet and Francois*, 2001; *Karsh et al.*, 2003; *DiFiore et al*., 2006]. Nitrogen is not lost or gained from the ocean during algal NO_3^- assimilation, but the spatial separation between net assimilation and remineralization can cause a trend of decreasing $\delta^{15}NO_3^-$ with depth. Distinguishing between the different isotope effects remains a challenge, especially in regions where multiple N-transformational processes are occurring within close proximity.

This study adds a dynamic nitrogen isotope module to an existing global ocean-atmosphere-sea ice-biogeochemical model designed for millennial timescale simulations. We provide a detailed description of the nitrogen isotope model and an assessment of its skill in reproducing present day $\delta^{15}NO_3^-$ observations. Comparison of model results with $\delta^{15}N$ observations will also be used to help to quantify processes that affect the global oceanic distribution of $\delta^{15}N$. Sensitivity experiments illustrate

the individual isotope effects of different processes on the spatial distribution of the N isotopes. In combination with measurements in ocean sediments and in the water column, the model can be a tool to better understand variations of $\delta^{15}N$ and the nitrogen cycle in the past and present.

2. Model Description

2.1 Physical Model

The physical model is based on the University of Victoria Earth System Climate Model [*Weaver et al.*, 2001], version 2.8. It includes a global, three-dimensional general circulation model of the ocean (Modular Ocean Model 2) with physical parameterizations such as diffusive mixing along and across isopycnals, eddy induced tracer advection [*Gent and McWilliams*, 1990] and a scheme for the computation of tidally induced diapycnal mixing over rough topography [*Simmons et al.*, 2004]. Nineteen vertical levels are used with a horizontal resolution of 1.8ºx3.6º. To improve the simulation of equatorial currents, we have increased the meridional resolution in the tropics to 0.9º (between 10ºS and 10ºN and smoothly transitioning to 1.8º at 20ºN/S) and added an anisotropic viscosity scheme [*Large et al.*, 2001]. A more detailed description of this parameterization and its effect on the equatorial circulation is provided in Supplementary Material 1. To account for the overestimated ventilation in the North Pacific, an artificial stratifying force equal to 0.05 Sv of freshwater is applied over the surface north of 55° in the Pacific and compensated elsewhere. A two dimensional, single level energy-moisture balance model of the atmosphere and a state-of-the-art dynamic-thermodynamic sea ice model are used, forced with prescribed NCEP/NCAR monthly climatological winds.

2.2 Marine Ecosystem Model

The marine ecosystem model is an improved version of the NPZD (Nutrient, Phytoplankton, Zooplankton, Detritus) ecosystem model of *Schmittner et al.* [2008] (Figure 1). The organic variables

include two classes of phytoplankton, N_2-fixing diazotrophs (P_D) and a NO_3^- assimilating algal phytoplankton class (P_A), as well as zooplankton (Z) and organic detritus (D). The inorganic variables include dissolved oxygen (O_2) and two nutrients, nitrate (NO_3^-) and phosphate (PO_4^{3-}), both of which are consumed by phytoplankton and remineralized in fixed elemental ratios ($R_{N:P}$ = 16, $R_{O:P}$ = 170). We note, though, that diazotrophs have been found to have $R_{N:P}$ as high as 50:1 (e.g., *Letelier and Karl*, [1996, 1998]). This simplification is one of the reasons why the nitrogen surplus $N' = NO_3^- - 16PO_4^{3-}$ is generally underestimated in surface waters in the model (Figure S2-1). In addition to water column denitrification and N_2 fixation, we now include a parameterization for sedimentary denitrification (see Supplementary Material 2, equation S2-11 and Figure 2), based on the flux of organic carbon into the sea floor sediments [*Middleburg et al.*, 1996]. Since the model underestimates coastal upwelling, which drives large fluxes of organic carbon to the sea floor sediments, this parameterization is tuned to fit the global mean $\delta^{15}NO_3^-$ observations. The complete marine ecosystem model description is provided in Supplementary Material 2. A comparison of the global distribution of NO_3^-, O_2, and N' with World Ocean Atlas 2005 (WOA05) observations is shown in Figure S2-1.

Water column denitrification is present in three main locations of the present-day oceans: the Eastern Tropical North Pacific (ETNP), the Eastern Tropical South Pacific (ETSP) and the Arabian Sea. Deficiencies in the physical circulation model simulate suboxic water in only one of these locations, the ETNP (Figure S2-1b). The physical circulation model integrates coastal upwelling over a horizontal extent that is too large (due to its coarse resolution), which results in the underestimation of upwelling, export production, and the remineralization of organic matter at depth. This bias leads to too high O_2 concentrations, larger than required for water column denitrification, in the ETSP and the Arabian Sea. Suboxia in the so-called “shadow zone” of the ETNP is simulated better and investigated more in Section 4.2. In the model, some water column denitrification also occurs in the Bay of Bengal

and off SW Africa (Figure 2C), which has not been observed in the real ocean. However, the anammox reaction, which also eliminates fixed-N in the water column, has been found to occur off SW Africa [*Kuypers et al.*, 2005, 2006]. *Navqi et al.* [1996] measured low decomposition rates in the Bay of Bengal. Effective ballasting and scavenging of organic matter by the massive riverine input of terrestrial matter, an effect not included in the model, may prevent water column denitrification in the Bay of Bengal, which is close to suboxic.

Diazotroph's grow according to the same principles as algal phytoplankton in the model (see Supplementary Material 2), but we also account for some of their different characteristics. N_2 fixation breaks down of the triple N bond of N_2, which is energetically more costly than assimilating fixed-N. Therefore, in the model, the growth rate of diazotrophs is lower than that of algal phytoplankton. It is zero in waters cooler than 15°C and increases 50% slower with temperature than the growth rate of algal phytoplankton. Diazotrophs are not limited by NO_3^- and will thrive in waters that are N-deficient (i.e., low N' as a result of denitrification) in which sufficient P and Fe are available. Denitrification and the propagation of N-deficient waters into the shallow thermocline by physical transport processes creates an ecological niche for diazotrophs in the model, which stimulates N_2 fixation [*Tyrell*, 1999].

One of the most important and best studied diazotrophs, *Trichodesmium*, also has large iron (Fe) requirements for growth [*Sanudo-Willhelmy et al.*, 2001]. Diazotrophs may depend on aeolian Fe in oligotrophic waters because deep pycnocline inhibits upward mixing of subsurface Fe-replete waters into the euphotic zone [*Letelier and Karl*, 1996; *Falkowski*, 1997]. Therefore, their growth rate is reduced by an additional 50% where estimated rates of aeolian dissolved Fe deposition are very low (< ~10 μmol m^{-2} yr^{-1}) (Figure 2A), primarily throughout the Tropical South Pacific [*Fan et al.*, 2006]. This is a simple parameterization of Fe limitation of diazotrophy and its full effects are described

elsewhere [*Somes*, 2009; *Somes and Schmittner*, in prep.]. The majority of N_2 fixation in the model occurs in oligotrophic waters 'downstream' of denitrification zones where sufficient Fe exists (i.e., via aeolian Fe deposition) (Figure 2B). The pattern of N_2 fixation—such as high values in the tropical/subtropical North Pacific, the western tropical/subtropical South Pacific, the western tropical/subtropical South Atlantic, the tropical/subtropical North Atlantic and the Indian Ocean—is mostly consistent with direct observations (e.g. *Karl et al.*, [2002]), with estimates based on the observed NO_3^- deficit and simulated circulation [*Deutsch et al.*, 2007], as well as with results from a more complex ecosystem model [*Moore et al.*, 2007]. However, N_2 fixation in our model does not extend northward of 20–25°N in the North Pacific and North Atlantic, whereas some observations show N_2 fixation as far north as 35–40°N.

2.3 Nitrogen Isotope Model

The nitrogen isotope model simulates the distribution of the two stable nitrogen isotopes, ^{14}N and ^{15}N, in all N species throughout the global ocean that are included in the marine ecosystem model. Five prognostic variables of $\delta^{15}N$ are embedded within the marine ecosystem model for all species containing nitrogen: NO_3^-, diazotrophs, algal phytoplankton, zooplankton and organic detritus (Figure 1). The 'isotope effect' is referred to in the following as the effect that each process has on the respective oceanic isotopic N pool, which depends on the $\delta^{15}N$ value of the substrate, the process-specific enrichment factor (ε), and the degree of utilization ($u_{substrate}$) of the substrate during the reaction:

$$\delta^{15}N_{product} = \delta^{15}N_{substrate} - \varepsilon(1 - u_{substrate}) \quad (2)$$

where $u_{substrate}$ is the fraction of the initial substrate used in the reaction. For example, if all of the

available substrate is consumed in the reaction (i.e., $u_{substrate} = 1$), the product will incorporate the $\delta^{15}N$ value of the substrate, nullifying any potential fractionation. However, if the rate of utilization is low (i.e., $u_{substrate} \sim 0$), the product will incorporate a relatively light $\delta^{15}N$ value compared to the substrate by the designated enrichment factor (Table 1).

The processes in the model that fractionate nitrogen isotopes are algal NO_3^- assimilation (ε_{ASSIM} = 5‰), zooplankton excretion (ε_{EXCR} = 6‰), and water column denitrification (ε_{WCD} = 25‰) (Table 1). Fractionation results in the isotopic enrichment of the more reactive, thermodynamically preferred, light ^{14}N into the product of each reaction by a process-specific fractionation factor. For a detailed discussion of nitrogen isotope fractionation dynamics see *Mariotti et al.* [1981]. Although little fractionation occurs during N_2 fixation in the model, it has an important effect on $\delta^{15}N$ by introducing relatively light atmospheric N_2 ($\delta^{15}N$ = 0‰) into the oceanic fixed-N inventory. Sedimentary denitrification also has been observed to have little effect on the oceanic isotopic N pool because denitrifiers consume nearly all NO_3^- diffusing into the sediments [*Brandes and Devol*, 1997, 2002; *Lehmann et al.*, 2004, 2007]. In the model, there is no fractionation during sedimentary denitrification (ε_{SD} = 0‰), although this is a simplification of observations [*Lehmann et al.*, 2007]. Fractionation during the remineralization of organic matter is not included in the model. The complete nitrogen isotope model description is provided in Appendix A.

3. Nitrogen Isotope Model Results

The model simulates complex spatial patterns of $\delta^{15}NO_3^-$ and $\delta^{15}N$-organic matter (OM) throughout the global ocean (top panels of Figure 3). Patterns of surface $\delta^{15}NO_3^-$ and subsurface $\delta^{15}N$-OM are very similar but values are offset by two processes. First, as much as 5‰ offset due to fractionation during NO_3^- uptake by phytoplankton and second, by fractionation during zooplankton excretion, which

increases the δ^{15}N-OM through zooplankton mortality (Figure 1). High δ^{15}N values (>15‰) are simulated in the eastern subtropical gyres, where surface NO_3^- is depleted, and in regions in close proximity to simulated suboxic zones in the Eastern Pacific, Bay of Bengal, and Eastern Atlantic (again, note that water column denitrification is has not been observed in the Bay of Bengal and Eastern Atlantic). A clear inter-hemispheric asymmetry appears between the subtropical gyres of the Pacific and Atlantic with higher values of 14-20‰ simulated in the southern hemisphere and smaller values of 10-14‰ in the northern hemisphere. More intermediate δ^{15}N values of 4 − 8‰ are found at high latitudes and near the equator where nutrient utilization is incomplete. δ^{15}N minima (<4‰) are located in the western tropical/subtropical ocean basins, where N_2 fixation occurs in the model (Figure 2B). The remainder of this section presents a more quantitative description of the contributions of individual processes to these relatively complex spatial patterns of $\delta^{15}NO_3^-$ and δ^{15}N-OM.

Figure 3 illustrates results from the full model (CTRL) that includes all isotope effects (top panels) together with results from sensitivity experiments designed to isolate the effects of individual processes (bottom panels) on the global δ^{15}N distribution . This is accomplished by removing the isotope effect of one process per experiment and then calculating the difference ($\Delta\delta^{15}$N) with CTRL. In the "NO_3^- Assimilation" and "Excretion" experiments, the enrichment factors ε_{ASSIM} and ε_{EXCR}, respectively, are set to zero. In the "N_2 fixation" experiment the diazotroph's N isotope ratio is set equal to that of other phytoplankton at each location. In the "Water Column Denitrification" and "Sedimentary Denitrification" experiments, the entire process is switched off (thereby changing the global N inventory). These latter experiments also show the indirect effect that both denitrification processes have on δ^{15}N through the stimulation of N_2 fixation. In all other isotope effect experiments, the total N inventory does not change.

3.1 Algal NO_3^- Assimilation

As phytoplankton preferentially assimilate $^{14}NO_3^-$ into organic matter, they leave the residual inorganic N pool enriched in $^{15}NO_3^-$, which creates an offset up to 5‰ between surface $\delta^{15}NO_3^-$ and surface δ^{15}N-OM that sinks towards the sea floor ("NO_3^- Assimilation" experiment, Figure 3). The surface NO_3^- utilization effect depends on the extent to which NO_3^- is consumed with respect to its physical supply. When NO_3^- utilization is low, which occurs in High Nitrate Low Chlorophyll (HNLC) regions such as the Southern Ocean, the northern North Pacific, and the eastern equatorial Pacific, surface $\delta^{15}NO_3^-$ is controlled mainly by the source of $\delta^{15}NO_3^-$ being supplied to the surface. Algae will fractionate NO_3^- during assimilation near their given enrichment factor in these N-replete waters so that the expected 5‰ difference between $\delta^{15}NO_3^-$ and δ^{15}N-OM is almost fully expressed (i.e., $\delta^{15}P_A = \delta^{15}NO_3^- - \varepsilon_{ASSIM}$ with $u_{ASSIM} \approx 0$ in Equation 2). Thus, NO_3^- utilization in HNLC regions has a small effect on surface $\delta^{15}NO_3^-$ but has a much larger effect on δ^{15}N-OM. This is perhaps most obvious in the Southern Ocean and in the northern North Pacific where $\Delta\delta^{15}NO_3^-$ is small, whereas $\Delta\delta^{15}$N-OM is strongly negative..

A different response is observed in oligotrophic regions where surface NO_3^- is depleted. Once the algae consume nearly all available NO_3^- (which itself becomes enriched in ^{15}N), they acquire the same N isotope signature from the source NO_3^- (i.e., $\delta^{15}P_A = \delta^{15}NO_3^-$ with u_{ASSIM} approaching 1). This drives the high δ^{15}N values in both NO_3^- and OM in the subtropics with maxima in the eastern poleward edges of the gyres (Figure 3). Although $\delta^{15}NO_3^-$ values are very high there, they have a small effect on δ^{15}N elsewhere because NO_3^- concentrations are very low. For instance, when low NO_3^- water mixes with nearby water with significantly higher NO_3^-, the resulting $\delta^{15}NO_3^-$ value will be weighted towards the water parcel containing more NO_3^- (see also *Deutsch et al.*, [2004]). This 'dilution effect' prevents high $\delta^{15}NO_3^-$ values in regions with high surface NO_3^- utilization from having

276 a large impact on the $\delta^{15}NO_3^-$ signature across the nitracline.

277

278 **3.2 Denitrification**

279 Water column denitrification only occurs at depth but its isotope effect can reach the surface due to
280 upwelling and vertical mixing of water enriched in $^{15}NO_3^-$. It has a large enrichment factor and
281 displays a very strong N isotope effect in close proximity to the simulated suboxic zones in the Eastern
282 Pacific, Bay of Bengal, and Eastern Atlantic ("Water Column Denitrification" experiment in Figure 3).
283 The unresolved poleward undercurrents along the western continental margin of the Americas—which
284 could, in the real world, propagate high $\delta^{15}NO_3^-$ away from the subsurface suboxic zones [*Kineast et*
285 *al.*, 2002]—may restrict the simulated water column denitrification isotope effect too much to regions
286 proximal to the suboxic zones. Both water column and sedimentary denitrification also indirectly lead
287 to lower $\delta^{15}NO_3^-$ values "downstream" of denitrification zones by creating more N-deficient water,
288 which stimulates additional N_2 fixation. This negative feedback also decreases the horizontal extension
289 of high $\delta^{15}NO_3^-$ signature originating from suboxic zones, because N_2 fixation introduces much lower
290 $\delta^{15}N$ into the ocean.

291

292 **3.3 N_2 Fixation**

293 The addition of newly fixed, isotopically light atmospheric N_2 ($\delta^{15}N_2 = 0$) by diazotrophs is the reason
294 for the low $\delta^{15}N$ values in the western tropical/subtropical ocean basins. Since denitrification is the
295 only process in the model that creates N-deficient water, and therefore an ecological niche for
296 diazotrophs, the majority of N_2 fixation in the model occurs "downstream" of denitrification zones after
297 phytoplankton have consumed all remaining surface NO_3^- and where sufficient aeolian Fe deposition
298 exists. This low $\delta^{15}NO_3^-$ signature is evident in the subtropical North/South Pacific, the subtropical
299 North/South Atlantic, and the Bay of Bengal ("N_2 Fixation" experiment, Figure 3).

300

301 **3.4 Excretion**

302 According to our model results, the N isotope effect of excretion has a smaller influence on the
303 simulated distribution of $\delta^{15}N$ in the global ocean ("Excretion" experiment, Figure 3) compared to the
304 other processes discussed above. Its strongest effect is observed in the subtropical South Pacific, where
305 NO_3^- is very low and excretion significantly contributes to the NO_3^- pool by introducing relatively low
306 $\delta^{15}NO_3^-$. Low latitude surface waters elsewhere are generally about 1-4‰ lighter due to fractionation
307 during excretion, with little spatial gradients. At high latitudes the effect on $\delta^{15}NO_3^-$ is very small. We
308 note that this N isotope effect is sensitive to the parameterization for excretion used in this marine
309 ecosystem model version. The excretion rate was tuned so that $\delta^{15}N$-zooplankton is enriched by ~3.4‰
310 relative to phytoplankton [*Minagawa and Wada*, 1984].

311

312 **4. Model Evaluation**

313 The relatively small number of $\delta^{15}N$ observations and the sparse spatial and temporal coverage make a
314 full global model assessment difficult. However, certain regions have been sampled sufficiently to
315 provide a meaningful comparison with the model results. All observations presented here are
316 interpolated horizontally onto a 0.9° x 1.8° grid using a Gaussian weighted algorithm. The 33 depth
317 levels are consistent with WOA05 and a linear interpolation is used for depths of missing data if nearby
318 data exist. A global database of $\delta^{15}NO_3^-$ measurements has thus been constructed and is available for
319 download (http://mgg.coas.oregonstate.edu/~andreas/Nitrogen/n15database.html). Figure 4 shows the
320 annually averaged global distribution of measured $\delta^{15}NO_3^-$, averaged over 200 – 300 m depth to
321 illustrate the spatial coverage. Seasonal sampling biases exist depending on the region. More details on
322 the data sets can be found in the respective ocean-region subsections that follow. Comparisons are
323 presented for the Southern Ocean (Indian-Pacific sector), the Eastern Tropical North Pacific, the

Central Equatorial Pacifc and the Subtropical North Atlantic. Other regions with available $\delta^{15}NO_3^-$ observations included in the dataset but not discussed in the text are the Bering Sea [*Lehmann et al.*, 2005], the Northeast Pacific [*Galbraith*, 2006], the Arabian Sea [*Altabet et al.*, 1999] and the eastern Pacific sector of the Southern Ocean [*Sigman et al.*, 1999].

Global measures of model performance for $\delta^{15}NO_3^-$ are presented in Table 2. These measures should be interpreted taken into account the highly localized nature of some of the processes as well as the limited regions covered by the database. A displacement in the location of denitrification, for example, will lead to a large decrease in the correlation coefficient and a large increase in the *RMS* errors. The CTRL model has a correlation coefficient of 0.68, implying that the model explains 46% of the variance in the observations. The decrease of the correlation coefficient and the increase of the *RMS* error due to the neglection of a particular process can be regarded as the importance that this process plays in explaining the global $\delta^{15}NO_3^-$ observations of the database. The correlation coefficient measures the pattern of variability and neglects the absolute values, whereas the *RMS* error considers the deviation of the model from the observations in absolute values. Neglecting water column denitrification leads to the largest decrease in the correlation coefficient to 0.29 and to the second largest increase in the *RMS* error after N_2 fixation. Neglecting algal NO_3^- assimilation also leads to a large decrease in the correlation coefficient and to a large increase in the *RMS* error. If N_2 fixation or sedimentary denitrification is not included, then the correlation coefficients decrease similarly, but exclusion of N_2 fixation causes a larger increase in the *RMS* error relative to sedimentary denitrification. Excretion has the weakest effect on the observed $\delta^{15}NO_3^-$ distribution in the model. Then, according to these measures, water column denitrification is the most important process determining the global $\delta^{15}NO_3^-$ distribution of the database, followed by algal NO_3^- assimilation. N_2 fixation is more important than sedimentary denitrification, whereas excretion is the least important.

348

349 **4.1 Southern Indian-Pacific Ocean**

350 The Southern Ocean represents a critical region of biogeochemical cycling in the ocean because it is
351 the largest open ocean region with incomplete drawdown of the major nutrients. This results in an
352 excess amount of CO_2 at the surface, which is released to the atmosphere (under pre-industrial
353 conditions). The degree to which surface nutrients are utilized here may have profound impacts on
354 ocean-atmosphere exchanges of CO_2. Figure 5 shows a comparison with observations recorded in the
355 region [*Sigman et al.*, 1999; *Altabet and Francois*, 2001; *DiFiore et al.*, 2006]. This data sub-set
356 compiles observations from 8 cruises covering various seasons. Since all cruises do not cover the same
357 location, some seasonal biases can be expected, yet, we still decided to use annual averages for
358 maximum spatial coverage. The model does not simulate interannual variability due to the prescribed
359 monthly climatological winds and temporally constant biogeochemical parameters.

360

361 Qualitatively, the inverse trend of increasing $\delta^{15}NO_3^-$ with decreasing NO_3^- (Figure 5a) is reproduced
362 by the model. However, the slope is underestimated suggesting that the enrichment factor for algal
363 NO_3^- assimilation used in the model (ε_{ASSIM} = 5‰) is too low, in agreement with *DiFiore et al.* [2006]
364 that suggests at least 7‰. The simulated vertical gradient is in good agreement with the observations.
365 Deep water $\delta^{15}NO_3^-$ at 2000 m depth is around 5‰ and slowly increasing throughout the lower
366 pycnocline to around 6‰ at 500 m depth. The model slightly overestimates $\delta^{15}NO_3^-$ between 200 m
367 and 400 m depth, whereas near surface values are slightly underestimated.

368

369 A large discrepancy between simulated and observational $\delta^{15}NO_3^-$ is apparent in surface waters north
370 of 40°S off the southern coast of Australia (Figure 5c). This bias is due to the fact that the model
371 overestimates the utilization of surface NO_3^- relative to observations there (Figure 5c). Where the

simulated NO_3^- is almost completely consumed (i.e., $NO_3^- < 1$ μM) (see Figure 5c-contour line), the remaining $\delta^{15}NO_3^-$ values become as high as 18‰. Since none of the existing $\delta^{15}NO_3^-$ observations was collected in such low NO_3^- concentrations (Figure 5a), it impossible, at this time, to falsify this aspect of the N isotope model response. We note this heavy $\delta^{15}NO_3^-$ signature in these low NO_3^- waters has little effect on $\delta^{15}NO_3^-$ across the nitracline in the model because the $\delta^{15}N$ signature of very low NO_3^- water becomes diluted out as it mixes with much higher NO_3^- water (see Section 3.1).

4.2 Eastern Tropical North Pacific

The ETNP contains the largest suboxic zone in the ocean, where water column denitrification occurs. The relatively small spatial scale of suboxic zones makes them difficult for the model to simulate accurately and deficiencies in the coarse resolution physical model prevent it from fully resolving some important physical processes, especially in coastal regions. Underestimating coastal upwelling (due to coarse resolution) results in corresponding underestimation of primary production, organic matter remineralization, and O_2 consumption at depth. This is a major reason for overestimated dissolved O_2 at depth in areas with significant coastal upwelling (e.g., off Peru and NW Mexico) (Figure S2-1), too large for water column denitrification to occur. Preliminary experiments suggest that increased vertical resolution can improve the simulation of productivity and suboxia in the Eastern Tropical South Pacific (not shown).

The ability to reproduce the equatorial undercurrents that transport relatively oxygen-rich water from the western basin is also important for the simulation of the Eastern Pacific suboxic zones. The anisotropic viscosity scheme [*Large et al.*, 2001] improves equatorial dynamics considerably (Supplementary Material 1). The Pacific Equatorial Undercurrent increases from 0.15 m/s to nearly 0.8 m/s, just slightly weaker than observations, which show velocities near 1 m/s (Figure S1-2). The North

Equatorial Countercurrent in the model also displays lower current velocities than observed, and does not deliver enough oxygen-rich water directly to the ETNP suboxic zone. This is likely the main reason why the simulated suboxic zone is much larger than observed towards the equator (Figures 6c).

Figure 6 shows model $\delta^{15}NO_3^-$ compared to observational $\delta^{15}NO_3^-$ data collected during November 1999 [*Sigman et al.*, 2005] and October 2000 [*Altabet*, previously unpublished]. The model captures the general observed trend of increasing $\delta^{15}NO_3^-$ as NO_3^- is consumed during water column denitrification (Figure 6a). The model's too low N:P ratio for diazotrophs may partly explain its incapacity to simulate some of the relatively high N' values of observations. The range of simulated values is also likely to be more limited compared to the observations due to the missing interannual and synoptic climate variability in the model.

Due to the described shortcomings in the physical circulation, the simulated suboxic zone is too large and located too far south (by ~5°) relative to observations (Figure 6c-contour line). This results in higher rates of water column denitrification and higher $\delta^{15}NO_3^-$ values, as well as more N-deficient water in the suboxic zone compared to observations. Figure 6b compares the horizontally averaged $\delta^{15}NO_3^-$ depth profiles only within the hypoxic zone ($O_2 < 10$ μM) at 300 m (contoured on Figure 6c) to account for the displaced OMZ. Within this region, the model is able to capture the general vertical distribution of $\delta^{15}NO_3^-$ seen in the measured data, such as the surface minimum and subsurface maximum.

$\delta^{15}NO_3^-$ in the ETNP decreases towards the surface [*Cline and Kaplan*, 1975; *Brandes et al.*, 1998; *Voss et al.*, 2001; *Sigman et al.*, 2005] suggesting a source of isotopically light N at the surface. *Brandes et al.* [1998] proposed that in the Arabian Sea as much as 30% of primary production must be

supported by N_2 fixation in order to account for the low surface $\delta^{15}NO_3^-$. Other observations also suggest that the decrease in $\delta^{15}NO_3^-$ towards the surface is likely due to the fixation of atmospheric N_2 and the subsequent, closely coupled remineralization-nitrification cycle [*Sigman et al.*, 2005]. We test this hypothesis by comparing the observations with the model experiment in which the isotope effect of N_2 fixation is neglected ("No NFIX"). In this case, the model overestimates surface $\delta^{15}NO_3^-$ by ~10‰ (Figure 6b) and the surface minimum is not simulated. This experiment demonstrates that the input of isotopically light fixed-N from N_2 fixation in the model best explains the decreasing trend of $\delta^{15}NO_3^-$ observations towards the surface. In the model, 20% of the fixed-N loss via denitrification is re-introduced into the surface by N_2 fixation occurring directly above the denitrification zone in the ETNP. The fact that the difference between the subsurface maximum and the near surface minimum is underestimated in the model (4‰ versus 8‰ in the observations) suggests that in the real world the locally re-introduced fraction could be larger than 20%.

4.4 North Atlantic

Uncertainties regarding processes that can affect the nitrogen isotope signal make it challenging to interpret and simulate nitrogen isotopes in the North Atlantic. Estimates of atmospheric N deposition [*Duce et al.*, 2008] and the assimilation-remineralization-nitrification cycle are not well constrained. Although atmospheric N deposition may be significant in this region [*Michaels et al.*, 1996; *Lipschultz et al.*, 2002; *Hansell et al.*, 2004, 2007; *Knapp et al.*, 2005, 2008], its isotopic composition is not well known and therefore is not included in the model at this time. Figure 7 shows the comparison of annual model $\delta^{15}NO_3^-$ with available observations from cruises in May 2001, 2004 [*Altabet and Montoya*, previously unpublished], October 2002 [*Knapp et al.*, 2008], and May 2005 [*Bourbounnais et al.*, 2009]. The model overestimates the $\delta^{15}NO_3^-$ values everywhere, by 0.9‰ on average and by 2‰ at 200 m depth, presumably due mostly to the underestimation of N_2 fixation, but possibly also because atmospheric N deposition and/or fractionation during the remineralization of organic matter

445 are not included. Both of these processes would act to decrease subsurface values of $\delta^{15}NO_3^-$.
446 Underestimated N' in the North Atlantic (Figure S2-1) also indicates too little N_2 fixation, but we again
447 note the too low N:P ratio for diazotrophs also contributes to this N' underestimation to some degree.
448
449 N_2 fixation is most likely underestimated in the model because it does not consider dynamic elemental
450 cycling of the microbial loop. It has been suggested that DOP is more labile relative to DON and
451 recycles through the microbial loop more efficiently, which can help relieve diazotrophs of P limitation
452 in this region [*Wu et al.*, 2000] and enhance N_2 fixation. The model is able to reproduce the pattern of
453 low $\delta^{15}NO_3^-$ in the thermocline qualitatively, just not quantitatively to the extent present in the
454 observations. Sedimentary denitrification in the North Atlantic stimulates enough N_2 fixation in the
455 model to generate a subsurface $\delta^{15}NO_3^-$ minimum. When sedimentary denitrification is switched off
456 ("No SD"), the thermocline minimum is not simulated. This suggests that sedimentary denitrification
457 is an important factor influencing N_2 fixation in the Subtropical North Atlantic, but not the only factor.
458
459 **5. Discussion and Conclusions**
460 A new model of nitrogen isotopes has been implemented into the three-dimensional ocean component
461 of a global Earth System Climate Model capable of millennial timescale simulations. Despite some
462 model deficiencies, we have shown that this model can successfully reproduce the general spatial
463 patterns of $\delta^{15}NO_3^-$ measured in the ocean. Sensitivity experiments allowed us to isolate the individual
464 N isotope effects of various N-transformational processes on the global distribution of $\delta^{15}N$. Algal
465 NO_3^- assimilation, water column denitrification, and N_2 fixation all have strong influences in setting
466 the global patterns of $\delta^{15}NO_3^-$ in the ocean, whereas the effect of zooplankton excretion is weaker.
467
468 These simulations show that the isotope effect of algal NO_3^- assimilation can drive very large spatial

gradients in both $\delta^{15}NO_3^-$ and δ^{15}N-OM depending on the ocean environment (Figure 3). In HNLC areas where surface NO_3^- utilization is low and algae are able to fractionate NO_3^- at their designated enrichment factor, the δ^{15}N-OM signature decreases. However, when NO_3^- utilization is high, the δ^{15}N-OM signature is more similar to the $\delta^{15}NO_3^-$ value it consumes because the effective degree of fractionation becomes much lower (see Section 3.1). Surface NO_3^- utilization gradients can transition rapidly, for example due to changes in ocean circulation, and can possibly drive large and rapid changes in $\delta^{15}NO_3^-$ and δ^{15}N-OM. The important influence of surface NO_3^- utilization on the global distribution of N isotopes in the model suggests that changes in surface NO_3^- utilization patterns throughout Earth's history could contribute to large fluctuations in δ^{15}N observed in sediment records, especially near fronts where large surface NO_3^- gradients exist (See also *Altabet and Francois* [1994]*; Farrell et al.* [1995]; *Francois et al.* [1997]; *Sigman et al.* [1999]; *Robinson et al.* [2005]; *Brunelle et al.* [2007]; *Galbraith et al.* [2008]).

The model simulates a strong direct and indirect isotope effect of denitrification. High $\delta^{15}NO_3^-$ produced by water column denitrification has clear regional impacts and is also responsible for overall elevated $\delta^{15}NO_3^-$ of the ocean relative to the N_2 fixation source (see below). The indirect effect of both water column and sediment denitrification is mediated by the production of N-deficient water, which creates an ecological niche for diazotrophs. This stimulates additional N_2 fixation when other suitable conditions for N_2 fixation also exist (e.g., warm (> 20°C), N-depleted water with sufficient P and Fe). This indirect effect also attenuates the horizontal circulation of high $\delta^{15}NO_3^-$ waters, originating from regions of water column denitrification, which causes its direct isotope effect to be regionalized to suboxic zones in the model.

Sedimentary denitrification also stimulates N_2 fixation, particularly over low latitude continental

493 shelves with high production. In the North Atlantic this effect is strong enough in the model to create a
494 subsurface $\delta^{15}NO_3^-$ minimum, which is improves the agreement with observations. Thus, N_2 fixation
495 in the ocean may be affected by the area of continental shelves (where the majority of the global
496 sedimentary denitrification occurs), which in turn is a function of global sea level [*Christensen et al.*,
497 1987; *Altabet and Curry*, 1989]. This suggests that glacial/interglacial changes in N_2 fixation in the
498 subtropical North Atlantic may have partly been driven by sea level change and its impact on
499 sedimentary denitrification (see also *Ren et al.*, [2009]).
500
501 Key features of the model have been identified that are in need of further development. The coarse
502 resolution physical circulation model does not fully resolve the dynamics of coastal upwelling regimes,
503 which in part drive the flux of organic matter towards the sea floor sediments and its remineralization
504 in the water column, as well as indirectly influences ventilation of suboxic zones. This is critical in the
505 simulation of water column denitrification and sedimentary denitrification, which are important
506 processes with respect to the global N isotope balance. Future model versions will include additional
507 vertical levels to better resolve continental shelves. The model neglects dynamic elemental
508 stoichiometry such as high N:P ratios of diazotrophs and the more efficient recycling of DOP relative to
509 DON in microbial loops, which can help relieve diazotrophs of their P limitation and allow them to fix
510 additional N_2 into the oceanic fixed-N pool in oligotrophic waters. The ecosystem model also suffers
511 from the exclusion of Fe as a prognostic tracer preventing it from being able to simulate differences in
512 ecosystems limited by marconutrients (NO_3^-, PO_3^{3-}) versus micronutrients (Fe).
513
514 Future applications of this model will include simulations of past climates, and direct comparison with
515 $\delta^{15}N$ sediment records will be used to test the model results. This approach may be a useful to
516 quantify past interactions between the marine N cycle and its isotopes, as well as their impact on

climate and may provide new insights into important physical and biogeochemical changes throughout Earth's history.

Appendix A. Nitrogen Isotope Model

The open system fractionation equation is used for fractionation during algal NO_3^- assimilation [*Altabet and Francois,* 2001]:

$$\delta^{15}P_O = \delta^{15}NO_3^- - \varepsilon_{ASSIM}(1 - u_{NO3}), \quad \text{(A1)}$$

where $\delta^{15}P_0$ is the δ^{15}N of phytoplankton biomass assimilated during one time step, Δt, and u_{NO3} is the fraction of NO_3^- available that is converted into biomass ($u_{ASSIM} = J_O P_O \times \Delta t / NO_3^-$). When algae assimilate all available NO_3^- into their biomass (i.e. $u_{ASSIM} = 1$) they will incorporate the same δ^{15}N value as that of the source material. Many studies have estimated the fractionation factor in both laboratory and ocean environments. A wide variety of values have been reported in culture settings ranging from 0.7‰ to 23‰ [*Wada and Hattori*, 1978; *Montoya and McCarthy*, 1995; *Waser et al.*, 1998; *Needoba et al.*, 2003; *Granger et al.*, 2004]. A more confined range has been observed in field estimates from 4‰ to 15‰ [*Wada,* 1980; *Altabet et al.*, 1991; *Altabet and Fracois*, 1994; *Wu et al.*, 1997; *Altabet et al.*, 1999; *Sigman et al.*, 1999; *Altabet and Francois*, 2001; *Karsh et al.*, 2003; *DiFiore et al.*, 2006; *Needoba et al.*, 2006] . In our model we choose a constant value of 5‰ which is near the majority of estimates, although it is important to bear in mind the uncertainty in the parameter choice and the possibility that it varies in space and time.

Nitrate in suboxic waters have been observed to have much higher δ^{15}N values due to fractionation during denitrification. Observations from present day suboxic zones in the Eastern Tropical North Pacific (ETNP) and the Arabian Sea (AS) have reported fractionation factors ranging from 22-30‰

[*Cline and Kaplan*, 1975; *Liu and Kaplan*, 1989; *Brandes et al.*, 1998; *Altabet et al.*, 1999; *Voss et al.*, 2001; *Sigman et al.*, 2003]; we adopt a value of 25‰ in the model. Note that because these estimates were derived from field studies in which the isotope effect was estimated from the total nitrogen loss, they implicitly include the effect of anammox [*Galbraith et al.*, 2008]. Fractionation during denitrification is also simulated using the open system fractionation equation

$$\delta^{15}NO_3^{OX} = \delta^{15}NO_3^- - \varepsilon_{WCD}(1 - u_{NO3}), \quad \text{(A2)}$$

where NO_3^{OX} is the oxygen-equivalent reduction of nitrate converted into N_2 gas during denitrification. The term u_{DENI} is the fraction of available NO_3 which is reduced into N_2 gas ($u_{NO3} = \mu_D D$ x *0.8* x $R_{O:N}$ x r^{NO3}_{sox} x L_{NO3} x Δt / NO_3).

Excretion is the process responsible for the step-wise enrichment of $\delta^{15}N$ along the trophic chain in our model and is simulated using the instantaneous fractionation equation:

$$\delta^{15}NO_3^- = \delta^{15}Z - \varepsilon_{EXCR}. \quad \text{(A3)}$$

The instantaneous fractionation equation is used because excretion will always be a small fraction of the total zooplankton biomass and has been measured to be depleted by ~6‰ relative to its body [*Montoya*, 2008], which is the source of the excreted nitrogen. This leads to the average enrichment of ~3.4 per trophic level [*Minagawa and Wada*, 1984].

Implementing these fractionation equations into the marine ecosystem model requires us to consider the exchanges of ^{14}N and ^{15}N between the various N pools separately. Total nitrogen abundance now

has the form

$$N = {}^{14}N + {}^{15}N \tag{A4}$$

for each variable in the isotope model. A fractionation coefficient is calculated for each process so the same equations for total N can be applied to ^{15}N [*Giraud et al.*, 2000]. For example, consider fractionation during algal NO_3^- assimilation. The isotopic ratio of new nitrogen biomass (P_O) is found using equations (1) and (2):

$$^{15}P_O = \beta_{ASSIM}\, {}^{14}P_O \tag{A5}$$

where

$$\beta_{ASSIM} = \frac{^{15}NO_3}{^{14}NO_3} - \frac{\varepsilon_{ASSIM}(1-u_{NO3})R_{std}}{1000}\,. \tag{A6}$$

Applying equations (C4) and (C5) gives the amount of new $^{15}P_O$ relative to the amount of total new nitrogen biomass, which is given by the primary production ($J_O P_O$), calculated by the marine ecosystem model.

$$^{15}P_O = \frac{\beta_{ASSIM}}{1+\beta_{ASSIM}} J_O P_O \tag{A7}$$

Analogous derivations can be done for all fractionation coefficients. The time-dependent set of equations for ^{15}N which are embedded into the marine ecosystem model are as follows:

589

590 $$\frac{\partial^{15}NO_3}{\partial t} = \left(R_D \mu_D D + \frac{\beta_{EXCR}}{1+\beta_{EXCR}} \gamma_2 Z + R_P \mu_P P_O - \frac{\beta_{ASSIM}}{1+\beta_{ASSIM}} J_O P_O - \frac{\beta_{ASSIM}}{1+\beta_{ASSIM}} u_N J_D P_D \right)$$

591 $$\times \left[1 - \frac{\beta_{WCD}}{1+\beta_{WCD}} 0.8 R_{O:N} r_{sox}^{NO3} L_{NO3} \right] \quad \text{(A8)}$$

592

593 $$\frac{\partial^{15}P_O}{\partial t} = \frac{\beta_{ASSIM}}{1+\beta_{ASSIM}} J_O P_O - R_P \mu_P P_O - R_{P_O} G(P_O) Z - R_{PO} \mu_{P2} P_O^2 \quad \text{(A9)}$$

594

595 $$\frac{\partial^{15}P_D}{\partial t} = \left(\frac{\beta_{ASSIM}}{1+\beta_{ASSIM}} u_N + \frac{\beta_{NFIX}}{1+\beta_{NFIX}} (1-u_N) \right) J_D P_D + -R_{P_D} G(P_D) Z - R_{P_D} \mu_P P_D \quad \text{(A10)}$$

596

597 $$\frac{\partial^{15}Z}{\partial t} = \gamma_1 \left[R_{P_O} G(P_O) + R_{P_D} G(P_D) \right] Z - \frac{\beta_{EXCR}}{1+\beta_{EXCR}} \gamma_2 Z - R_Z \mu_Z Z^2 \quad \text{(A11)}$$

598

599 $$\frac{\partial^{15}D}{\partial t} = 1 - \gamma_1 \left[R_{P_O} G P_O + R_{P_D} G P_D \right] Z + R_{P_D} \mu_P P_D + R_{P_O} \mu_{P2} P_O^2 + R_Z \mu_Z Z^2 - R_D \mu_D D - R_D w_D \frac{\partial D}{\partial z}$$

600 (A12)

601

602 where $R_{N=\text{PO, PD, Z, D}} = {}^{15}\text{N} / ({}^{14}\text{N} + {}^{15}\text{N})$ is the ratio of heavy over total nitrogen. The complete

603 parameter description is provided in Supplementary Material 2. Here it suffices to note that the

604 equations for total nitrogen (${}^{14}\text{N} + {}^{15}\text{N}$) are identical to the ones of ${}^{15}\text{N}$ except that $R_X = \beta_X/(1+\beta_X) = 1$

605 in the total nitrogen equations.

606

607 The model was carefully tested with zero fractionation in order to quantify and minimize numerical

608 errors, which can occur for example due to slightly negative values of biological tracers caused by

609 inaccuracies of the advection scheme. The biological code was adjusted to avoid negative
610 concentrations as much as possible. Initially numerical errors in $\delta^{15}N$ ranged from ± 1‰ in grid points
611 at the sea floor to ± 0.1‰ in the upper ocean. Setting $R_{std} = 1$ instead of $R_{std} = 0.0036765$, the actual
612 atmospheric N_2 isotope ratio, reduces the numerical errors by over an order of magnitude. R_{std} is set to
613 the value 1 so both isotope variables will be on the same order of magnitude. This prevents ^{15}N from
614 becoming very close to zero as often, where inaccuracies of the advection scheme can cause it to be
615 negative. This modification amounts to a scaling of ^{15}N and ^{14}N by a constant factor which does not
616 affect the $\delta^{15}N$ dynamics. The remaining numerical errors of ±0.1‰ in the deep ocean and ±0.01‰ in
617 the upper ocean are two orders of magnitude smaller than the observed variability. The model is
618 integrated for over 7,000 years as it approaches equilibrium.
619

References Cited

Abell, J., S. Emerson, and P. Renaud (2000), Distributions of TOP, TON and TOC in the North Pacific subtropical gyre: Implications for nutrient supply in the surface ocean and remineralization in the upper thermocline, *Journal of Marine Research, 58,* 203–222

Altabet, M. A., W. G. Deuser, S. Honjo, C. Stienen (1991), Seasonal and depth-related changes in the source of sinking particles in the North Atlantic, *Nature, 354*, 136-139

Altabet , M.A. and R. Francois (1994), Sedimentary nitrogen isotopic ratio as a recorder for surface ocean nitrate utiliztion, G*lobal Biogeochem. Cycles*, *8*, 103-116

Altabet, M. A., C. Pilskaln, R. Thunell, C. Pride, C. Sigman, F. Chavez, R. Francois (1999), The nitrogen isotope biogeochemistry of sinking particles from the margin of the Eastern North Pacific, *Deep-Sea Res. I., 46*, 655-679

Altabet, M. A., D. W. Murray and W. L. Prell (1999), Climate-linked variations in Arabian Sea denitrification over the last 1 m.y.: Implications for the marine N cycle, *Paleoceanogr., 14*, 732-743

Altabet, M. A., and R. Francois (2001), Nitrogen isotope biogeochemistry of the Antarctic Polar Frontal Zone at 170W, *Deep Sea Res. II., 48*, 4247-4273

Altabet, M. A. (2001), Nitrogen isotopic evidence for micronutrient control of fractional NO_3 utilization in the equatorial Pacific, *Limnol. Oceanogr., 46*(2), 368-380

Altabet, M. A. (2005), Isotopic tracers of the marine nitrogen cycle, In: *Marine Organic Matter: Chemical and Biological Markers* edited by J. Volkman, vol. 2 of "The Handbook of Environmental Chemistry", Editor-in-Chief: O. Hutzinger, pp. 251-293, http://dx.doi.org/10.1007/698_2_008

Altabet, M. A., Higginson, M., and Murray, D. W. (2007), The effect of millennial-scale changes in Arabian Sea denitrification on atmospheric CO_2, *Nature*, *415*, 159-162

Altabet, M. A. (2007), Constraints on oceanic N balance/imbalance from sedimentary ^{15}N records, *Biogeosciences*, *4*, 75-86

Berelson, W. M. (2002), Particle settling rates increase with depth in the ocean, *Deep-Sea Res., 49*, 237-251

Brandes, J. A., and A. H. Devol (1997), Isotopic fractionation of oxygen and nitrogen in coastal marine sediments, *Geochim. et Sosmo. Acta*, *61*(9), 1793-1801

Brandes, J. A., A. H. Devol, T. Yoshinari, D. A. Jayakumar, S. W. A. Naqvi (1998), Isotopic composition of nitrate in the central Arabian sea and eastern tropical pacific: A tracer of mixing and nitrogen cycles, *Limnol. Oceanogr., 43*(7), 1680-1689

Brandes, J. A, and A. H. Devol (2002), A global marine-fixed nitrogen isotopic budget: Implications for Holocene nitrogen cycling, *Global Biogeochem. Cycles*, *16*, 1120, doi:10.1029/2001GB001856

Bryan, K., S. Manabe, R. C. Pacanowski (1975), A global ocean-atmosphere climate model. Part II: The ocean circulation, *J. Phys. Oceanogr., 5*, 30-46

Bourbonnais, A., M. F. Lehmann, J. J. Waniek, and D. E. Schulz-Bull (2009), Nitrate isotope anomalies reflect N2 fixation in the Azores Front region (subtropical NE Atlantic), *Journal of Geophys. Res.*, *114*, C03003, doi:10.1029/2007JC004617

Capone, D. G., J. P. Zehr, H. Paerl, B. Bergman, and E. J. Carpenter (1997), *Trichodesmium*, a globally significant marine cyanobacterium, *Science, 276*, 1221-1229

Carpenter, D. G., H. R. Harvey, B. Fry, D. G. Capone (1997), Biogeochemical tracers of the marine cyanobacterium *Trichodesmium*, *Deep-Sea Res. I*, *44*, 27-38

Carpenter, E. J., J. P. Montoya, J. Burns, M. Mulholland, A. Subramanian, and D. G. Capone (1998), Extensive bloom of a N_2-fixing symbiotic association (*Hemiaulis hauckii* and *Richelia intracellularis*) in the tropical Atlantic Ocean, *Marine Ecology Progress Series*, *172***,** 281-292.

Checkley, Jr., D. M. and C. A. Miller (1989), Nitrogen isotope fractionation by oceanic zooplankton, *Deep Sea Res.*, *36*, 1449-1456

Cline, J. D. and I. R. Kaplan (1975), Isotopic fractionation of dissolved nitrate during denitrification in the eastern tropical North Pacific Ocean, *Mar. Chem.*, *3*, 271-299

Codispoti, L. A., and F. A. Richards (1976), An analysis of the horizontal regime of denitrification in the eastern tropical North Pacific, *Limnol. Oceanogr.*, *21(3)*, 379-388

Codispoti, L. A. (2007), An oceanic fixed nitrogen sink exceeding 400 Tg N a^{-1} vs the concept of homeostasis in the fixed-nitrogen inventory, *Biogeosciences*, *4*, 233-253

De Pol-Holz, R., O. Ulloa, L. Dezileau, J. Kaiser, F. Lamy, D. Hebbeln (2006), Melting of the Patagonian Ice Sheet and deglacial perturbations of the nitrogen cycle in the eastern South Pacific, *Geophy. Res. Lett.*, *33*, L04704, doi:10.1029/2005GL024477

Delaney, M. L. (1998), Phosphorus accumulation in marine sediments and the oceanic phosphorus cycle, *Blobal Biogeochem. Cycles*, *12*(4), 563-572

Deutsch, C., D. M. Sigman, R. C. Thunell, A. N. Meckler, G. H. Haug (2004), Isotopic constraints on glacial/interglacial changes in the oceanic nitrogen budget, *Global Biogeochem. Cycles*, *18*, GB4012, doi:10.1029/2003GB002189

Deutsch, C., J. L. Sarmiento, D. M. Sigman, N. Gruber, J. P. Dunne (2007), Spatial coupling of nitrogen inputs and losses in the ocean, *Nature*, *445*, doi:10.1038/nature05392

Delwiche, C. C. and P. L. Steyn (1970), Nitrogen isotope fractionation in soils and microbial reactions, *Envrion. Sci. Technol.*, *4*, 929-935

DiFiore, P. J., D. M. Sigman, T. W. Trull, M. J. Lourey, K. Karsh, G. Cane, R. Ho (2006), Nitrogen isotope constraints on subantarctic biogeochemistry, *J. Geophys. Res.*, *111*, C08016, doi:10.1029/2005JC003216

Emmer, E., and R. C. Thunell (2000), Nitrogen isotope variations in Santa Barbara Basin sediments: Implications for denitrification in the eastern tropical North Pacific during the last 50,000 years, *Paleoceanograhy*, *15*, 377-387

Falkowski, P. G. (1997), Evolution of the nitrogen cycle and its influence on the biological sequestration of CO_2 in the ocean, *Nature*, *387*, 272-275

Fan, S.-M., W. J. Moxim, H. L. Il (2006), Aeolian input of bioavailable iron to the ocean, *Geophys. Res. Letters*, *33*, L07602, doi:10.1029/2005GL024852

Fogel, M. L., and L. A. Cifuentes (1993), Isotope Fractionation during Primary Production. In: Engel, M.H. and A. Macko (Editors), *Organic Geochemistry*, Plenum Press, New York, pp. 861

Galbraith, E. D., M. Kinast, T. F. Pedersen, and S. E. Calvert (2004), Glacial-interglacial modulation of the marine nitrogen cycle by high-latitude O2 supply to the global thermocline, *Paleoceanography*, *19*, PA4007, doi:10.1029/2003PA001000

Galbraith, E (2006), Interactions between climate and the marine nitrogen cycle on glacial-interglacial time scales, Ph.D. thesis, University of British Columbia

Galbraith, E. D., M. Kienast, S. L. Jaccard, T. F. Pedersen, B. G. Brunelle, D. M. Sigman, and T. Kiefer (2008), Consistent relationship between global climate and surface nitrate utilization in the western subarctic Pacific throughout the last 500 ka, *Paleoceangr.*, *23*, PA2212, doi:10.1029/2007PA001518

Ganeshram, R. S., T. F. Pedersen, S. E. Calvert, J. W. Murray (1995), Large changes in oceanic nutrient inventories from glacial to interglacial periods, *Nature*, *376*, 755-758

Ganeshram, R. S., T. F. Pedersen, S. E. Calvert, G. W. McNeill, M. R. Fontugne (2000), Glacial-interglaical variability in denitrification in the World's Oceans: Causes and consequences, *Paleoceanogr.*, *15*, 361-376

Gaye-Haake, B., N. Lahajnar, L.-Ch. Emeis, D. Unger, T. Rixen, A. Suthhof, V. Ramaswamy, H. Schulz, A. L. Paropkari, M. V. S. Guptha, V. Ittekkot, (2005), Stable nitrogen isotope ratios of

716 sinking particles and sediments from the nothern Indian Ocean, *Mar. Chem.*, *96*(3-4), 243-255,
717 doi:10.1016/j.marchem.2006.02.001
718 Gent, P. R., and J. C. McWilliams (1990), Isopycnal mixing in ocean circulation models, *J. Phys.*
719 *Oceanogr.*, *20*, 150-155
720 Giraud, X., P. Bertrand, V. Garcon, I. Dadou (2000), Modeling δ15N evolution: First
721 palaeoceanographic applications in a coastal upwelling system, *J. Mar. Res.*, *58*, 609-630
722 Granger, J., D. M. Sigman, J. A. Needoba, and P. J. Harrison (2004), Coupled nitrogen and oxygen
723 isotope fractionation of nitrate during assimilation by cultures of marine phytoplankton, *Limnol.*
724 *Oceanogr.*, *49*(5), 1763-1773
725 Grantham, B. A., F. Chan, K. J. Nielsen, D. S. Fox, J. A. Barth, A. Huyer, J. Lubchenco and B. A.
726 Menge (2004), Nearshore upwelling-driven hypoxia signals ecosystem and oceanographic changes
727 in the NE Pacific, *Nature*, *429*, 749-754
728 Gruber, N. and J. L. Sarmiento (1997), Global patterns of marine nitrogen fixation and denitrification,
729 *Global Biogeochem. Cycles*, *11*, 235-266
730 Hansell, D.A., N.R. Bates (2004), Excess nitrate and nitrogen fixation in the North Atlantic, *Marine*
731 *Chemistry*, *84*, 243-265
732 Hansell, D. A., D. B. Olson, F. Dentener, L.M. Zamora (2007), Assessment of excess nitrate
733 development in the subtropical North Atlantic, *Marine Chem.*, *106*, 562-579
734 Hendy, I. L., T. F. Pedersen, J. P. Kennett, R. Tada (2004), Intermittent existence of a southern
735 Californian upwelling cell during submillennial climate change of the last 60 kyr,
736 *Paleoceanography*, *19*, PA3007, doi:10.1029/2003PA000965
737 Holl, C. M. and J. P. Montoya (2005), Interactions between nitrate uptake and nitrogen fixation in
738 continuous cultures of the marine diazotroph *Trichodesmium* (cyanobacteria), *J. Phycol.*, *41*(6),
739 1178-1183
740 Jackson, G. A. and P. M. Williams (1985), Importance of dissolved organic nitrogen and phosphorus to
741 biological nutrient cycling. *Deep- Sea Res.*, *32*, 223-235.
742 Jickells, T. D., Z. S. An, K. K. Andersen, A. R. Baker, G. Bergametti, N. Brooks, J. J. Cao, P. W. Boyd,
743 R. A. Duce, K. A. Hunter, H. Kawahata, N. Kubilay, J. laroche, P. S. Liss, N. Mahowald, J. M.
744 Prospero, A. J. Ridgwell, I. Tegen, R. Torres (2005), Global Iron Connections Between Desert
745 Dust, Ocean Biogeochemistry, and Climate, *Science*, *308*, 67-
746 Karl, D, A. Michaels, B. Bergman, D. Capone, E. Carpenter, R. Letelier, F. Lipschultz, H. Paerl, D.
747 Sigman, L. Stal (2002), Dinitrogen fixation in the world's oceans, *Biogeochemistry*, *57/58*, 47-98
748 Karsh, K. L., T. W. Trull, M. J. Lourey, and D. M. Sigman (2003), Relationship of nitrogen isotope
749 fractionation to phytoplankton size and iron availability during the Southern Ocean Iron RElease
750 Experiment (SOIREE), Limnol. Oceanogr., 48(3), 2003, 1058-1068
751 Kessler, W. S. (2006), The circulation of the eastern tropical Pacific: A review, *Progress in Oceanogr.*,
752 *69*, 181-217
753 Kineast, S. S., S. W. Calvert, T. F. Pedersen (2002), Nitrogen isotope and productivity variations along
754 the northeast Pacific margin over the last 120 kyr: surface and subsurface paleoceanography,
755 *Paleoceanogr.*, *17*(4), 1055, doi:10.1029/2001PA000650
756 Knapp, A. N., D. M. Sigman, F. Lipschultz (2005), N isotopic composition of dissolved organic and
757 nitrate at the Bermuda Atlantic Time-series Study site, *Global Biogeochem. Cycles*, *19*,
758 doi:10.1029/2004GB002320
759 Knapp, A. N., P. J. DiFiore, C. Deutch, D.M. Sigman, F. Lipschultz (2008), Nitrate isotopic
760 composition for N2 fixation in the Atlantic Ocean, *Global Biogeochem. Cycles*, *22*, GB3014,
761 doi:10.1029/2007GB003107
762 Kustka, A., E. J. Carpenter, and S. A. Sanudo-Wilhelmy (2002), Iron and marine nitrogen fixation:
763 Progress and future direction, *Res. Microbiol.*, *153*, 255-262

764 Kuypers, M. M. M., G. Lavik, D. Woebken, M. Schmid, B. M. Fuchs, R. Amann, B. B. Jorgensen, M.
765 S. M. Jetten (2005), Massive nitrogen loss from the Benguela upwelling system through anaerobic
766 ammonium oxidation, *Proc. Nat. Aca. Sci.*, *102*, 5478-5483
767 Kuypers, M. M. M., G. Lavik, B. Thamdrup (2006) Anaerobic ammonium oxidation in the marine
768 environment in: *Past and Present Water Column Anoxia*. *NATO Science Series*, IV. *Earth and*
769 *Environmental Sciences, 64*, edited by: L. Neretin, Springer, Dordrecht, 311-355
770 Large, W. C., G. Danabasoglu, J. C. McWilliams, P. R. Gent, F. O. Bryan (2001), Equatorial circulation
771 of a global ocean climate model with anisotropic horizontal visosity, *J. Phys. Oceanogr.*, *31*, 518-
772 536
773 Lehmann, M. F., S. M. Bernasconi, A. Barbieri, J. A. McKenzie (2002), Preservation of organic matter
774 and alteration of its carbon and nitrogen isotope composition during simulated and in situ early
775 sedimentary diagenesis, *Geochim. Cosmochim. Acta*, *66*(20), 3573-3584, doi:10.1016/S0016-
776 7037(02)00968-7
777 Lehmann, M. F., D. M. Sigman, and W. M. Berelson (2004), Coupling the 15N/14N and 18O/16O of
778 nitrate in benthic nitrogen cycling, *Marine Chemistry, 88*, 1 – 20
779 Lehmann, M. F., D. M. Sigman, D. C. McCorkle, B. G. Brunelle, S. Hoffmann, M. Kienast, G. Cane, J.
780 Clement (2005), Origin of the deep Bering Sea nitrate deficit: Constraints from the nitrogen and
781 oxygen isotopic composition of water column nitrate and benthic nitrate fluxes, *Global*
782 *Biogeochem. Cycles*, *19*, GB4005, doi:10.1029/2005GB0002508
783 Letelier, R. M. and D. M. Karl (1996), Role of Trichodesmium spp. in the productivity of the
784 subtropical North Pacific Ocean., *Mar. Ecol. Prog. Ser*, *133*, 263-273
785 Letelier, R. M. and D. M. Karl (1998), Trichodesmium spp. physiology and nutrient fluxes in the North
786 Pacific subtropical gyre. *Aquat. Microb. Ecol.*, *15*, 265-276
787 Lipschultz, F., N. R. Bates, C. A. Carlson, D. A. Hansell (2002), New production in the Sargasso Sea:
788 History and current status, *global Biogeochem. Cycles*, *16*(1), 1001, doi:10.1029/2000GB001319
789 Liu, K. K., and I. R. Kaplan (1989), the eastern tropical Pacific as a source of N-15 enriched nitrate in
790 seawater off southern California, *Limnol. Oceanogr., 34(5)*, 820-830
791 Luo, C., N. Mahowald, and J. del Corral (2003), Sensitivity study of meteorological parameters on
792 mineral aerosol mobilization, transport and distribution, *J. Geophys. Res.*, *108*(D15), 4447,
793 doi:10.1029/2003JD003483
794 Macko, S. A. M. L. Fogel, P. E. Hare, and T. C. Hoering (1987), Isotope fractionation of nitrogen and
795 carbon in the synthesis of amino acids by microorganisms, *Chem. Geol.*, *65*, 79-92
796 Mahowald, N. M., M. Yoshioka, W. D. Collins, A. J. Conley, D. W. Fillmore, and D. B. Coleman
797 (2006), Climate response and radiative forcing from mineral aerosols during the last glacial
798 maximum, pre-industrial, current and doubled-carbon dioxide climates, *Geophys. Res. Lett.*,
799 *33*(20), -, Artn L20705, Doi 10.1029/2006gl026126.
800 Mariotti, A., J. C. Germon, P. Hubert, P. Kaiser, R. Letolle, A. Tardieux, P. Tardieux (1981),
801 Experimental determination of nitrogen kinetic isotope fractionation: some principles; illustration
802 for the denitrification and nitrification processes, *Plant and Soil Science*, *62*, 413-430
803 Marland, G., T. A. Boden, and R. J. Andres (2006), In Trends: A Compendium of Data on Global
804 Change, Carbon Dioxide Information Analysis Center, Oak ridge National Laboratory, U.S.
805 Department of Energy, Oak Ridge, Tenn. USA
806 Matsumoto, K. et al. (2004), Evaluation of ocean carbon cycle models with data-based metrics,
807 *Geophys. Res. Lett.*, *31*, L07303
808 McElroy, M. B. (1982), Marine biological controls on atmospheric CO_2 and climate, *Nature*, *302*, 328-
809 329
810 Michaels, A. F., D. Olson, J. L. Sarmiento, J. W. Ammerman, K. Fanning, R. Jahnke, A. H. Knapp, F.
811 Lipschultz, J. M. Prospero (1996), Inputs losses and transformations of nitrogen and phosphorus in

812 the pelagic North Atlantic, In: Howarth, R. W. (Ed.), Nitrogen Cycling in the North Atlantic Ocean
813 and its Watersheds. Kluwer Academic Publishers, Boston, MA, pp. 181-226
814 Middleburg, J. J., K. Soetaert, P. M. J. Herman, and C. H. R. Heip (1996), Denitrification in marine
815 sediments: A model study, *Global Biogeochem. Cycles*, *10*(4), 661-673
816 Minagawa, M. and E. Wada (1984), Stepwise enrichment of 15N along food chains: Further evidence
817 and the relation between δ15N and animal age, *Geochimica et Cosmochimica Acta*, *48*, 1135-1140
818 Minagawa, M., and E. Wada (1986), Nitrogen isotope ratios of red tide organisms in the East China Sea
819 - a characterization of biological nitrogen fixation, *Mar. Chem*., *19(3)*, 245-259
820 Monnin, E., A. Indermuhle, A. Dallenbach, J. Fluckiger, B. Stauffer, T. F. Stocker, D. Raynaud, J.-M.
821 Barnola (2001), Atmospheric CO_2 Concentrations over the Last Glacial Termination, *Science*, *291*,
822 112-114
823 Montoya, J. P. and J. J. McCarthy (1995), Isotopic fractionation during nitrate uptake by phytoplankton
824 grown in continuos culture, *J. of Plankton Res.*, *17*(3), 439-464
825 Montoya, J. P., E. J. Carpenter, D. G. Capone (2002), Nitrogen fixation and nitrogen isotope
826 abundances in zooplankton of the oligotrophic North Atlantic, *Limnol. Oceanogr.*, *47*, 1617-1628
827 Moore, J. K. and S. C. Doney (2007), Iron availability limits the ocean nitrogen inventory stabilizing
828 feedbacks between marine denitrification and nitrogen fixation, *Global Biogeochem. Cycles*, *21*,
829 GB2001, doi:10.1029/2006GB002762
830 Munk, W. H. (1950), On the wind driven ocean circulation, *J. Meteor.*, *7*, 79-93
831 Naqvi, S. S. A. (2007), The Indian Ocean, in: Nitrogen in the the Marine Environment, edited by:
832 Capone, D. G., Bronk, D. A., Mulhollnad, M. R., and Carpenter, E. J., *Academic Press*
833 Needoba, J. A., N. A. Waser, P. J. Harrison, S. E. Calvert (2003), Nitrogen isotope fractionation in 12
834 species of marine phytoplankton during growth on nitrate, *Marine Ecology: Progress Series*, *255*,
835 81-91
836 Needoba, J. A. and Harrison, P. J. (2004) Influence of low light and a light:dark cycle on NO_3^- uptake,
837 intracellular NO_3^-, and nitrogen isotope fractionation by marine phytoplankton, *Journal of*
838 *Phycology*, *40*(3), 505-516
839 Postgate, J. (1998), Nitrogen Fixation 3rd edn 1-120 (Cambridge Univ. Press, Cambridge, 1998)
840 Raven, J. A., M. C. W. Evans, R. E. Korb (1999), The role of trace metals in photosynthetic electron
841 transport in O_2-evolving organisms, *Photosynth. Res.*, *60*, 111-149
842 Ren, H., D. M. Sigman, A. N. Meckler, B. Plessen, R. S. Robinson, Y. Rosenthal, G. H. Haug (2009),
843 Foraminiferal Isotope Evidence of Reduced Nitrogen Fixation in the Ice Age Atlantic Ocean,
844 *Science*, *323*, 244-248
845 Sanudo-Wilhelmy, S. A., A. B. Kustka, C. J. Gobler (2001), Phosphorus limitation by *Trichodesmium*
846 in the central Atlantic Ocean, *Nature*, *411*, 66-69
847 Sanudo-Wilhelmy, S. A., A. Tovar-Sanchez, F.-X. Fu, D. G. Capone, E. J. Carpenter, and D. A.
848 Hutchins (2004), The impact of surface-adsorbed phosphorus on phytoplankton Redfield
849 stoichiometry, *Nature*, *432*, 897-901
850 Schartau, M., and Oschlies, A. (2003), Simultaneous data-based optimization of a 1D-ecosystem model
851 at three locations in the North Atlantic: Part I-Method and parameter estimates, *J. Mar. Res.*, *61*,
852 765-793
853 Schmittner, A., A. Oschlies, X. Giraud, M. Eby, and H. L. Simmons (2005), A global model of the
854 marine ecosystem for long-term simulations: Sensitivity to ocean mixing, buoyancy forcing,
855 particle sinking, and dissolved organic matter cycling, *Glob. Biogeochem. Cycles*, *19*(3), GB3004,
856 doi: 10.1029/2004GB002283: doi:10.1029/2004GB002283.
857 Schmittner, A., E. D. Galbraith, S. W. Hostetler, T. F. Pedersen, R. Zhang (2007), Large fluctuations of
858 dissolved oxygne in the Indian and Pacific oceans during Dansgaard-Oeschger oscillations caused
859 by variations of North Atlantic Deep Water subduction, *Paleoceangr.*, *22*,

doi:10.1029/2006PA001384
Schmittner, A., A. Oschlies, H. D. Matthews, and E. D. Galbraith (2008), Future changes in climate, ocean circulation, ecosystems and biogeochemical cycling simulated for a business-as-usual CO2 emission scenario until year 4000 AD, *Global Biogeochem. Cycles*, *22*, GB1013, doi:10.1029/2007GB002953
Sigman, D. M., M. A. Altabet, R. Michener, D. D. McCorkle, B. Fry, R. M. Holmes (1997), Natural abundance-level measurement of the nitrogen isotopic composition of oceanic nitrate: Ann adaptation of the ammonia diffusion method, *Mar. Chem.*, *57*, 227-242
Sigman, D. M., M. A. Altabet, D. D. McCorkle, R. Francois, G. Fischer (1999), The δ15N of nitrate in the Southern Ocean: Consumption of nitrate in surface waters, *Global Biogeochem. Cycles*, *13*(4), 1149-1166
Sigman, D. M., R. Robinson, A. N. Knapp, A. van Green, D. C. McCorkle, J. A. Brandes, R. C. Thunell (2003), Distinguishing between water column and sedimentary denitrification in the Santa Barbara Basin usinkg the stable isotopes of nitrate, *Geochem., Geophys., Geosys.*, *4*(5), 1-20, doi:10.1039/2002GC00384
Sigman, D. M., J. Granger, P. J. DiFiore, M. M. Lehmann, R. Ho, G. Cane, A. van Green (2005), Coupled nitrogen and oxygen isotope measurements of nitrate along the eastern North Pacific margin, *Global Biogeochem. Cycles*, *19*, GB4022, doi:10.1029/2005GB0002458
Simmons, H. L., S. R. Jayne, L. C. St. Laurent, A. J. Weaver (2004), tidally driven mixing in a numerical model of the ocean general circulation, *Ocean Model.*, *6*, 245-263
Smith, S. V., W. J. Kimmerer, and T. W. Walsh (1986), Vertical flux and biogeochemical turnover regulate nutrient limitation of net organic production in the North Pacific Gyre, *Limnol. Oceanogr.*, *31*(1), 161-167
Somes, C. J. (2009), Nitrogen isotopes in a global ocean biogeochemical model: constraints on the couping between denitrification and nitrogen fixation, M.S. thesis, Oregon State University
Sutka, R. L., N. E. Ostrom, P. H. Ostrom, M. S. Phankumar (2004), Stable nitrogen isotope dynamics of idssolved nitrate in a transect from the North Pacific Subtropical Gyre to the Eastern Tropical North Pacific, *Geochimica et Cosmochimica Acta*, *68*(3), 517-527
Thamdrup, B., T. Dalsgaard, M. M. Jensen, O. Ulloa, L. Farias, R. Escribano (2006), Anaerobic ammonium oxidation in the oxygen-deficient waters off northern Chile, *Limnol. Oceanogr.*, *51*(5), 2145-1256
Thunell, R. C., D. M. Sigman, F. Muller-Karger, Y. Astor, R. Varela (2004), Nitrogen isotope dynamics of the Cariaco Basin, Venezuela, *Global Biogeochem. Cycles*, *18*, GB3001, doi:10.1039/2003GB002185
Tyrell, T. (1999), The relative influence of nitrogen and phosphorus on oceanic primary production, *Nature*, *400*, 525-531
Voss, M. J., J. W. Dippner, J. P. Montoya (2001), Nitrogen isotope patterns in the oxygen deficient waters of the Eastern Tropical North Pacific Ocean, *Deep Sea Res. I*, *48*(8), 35-49
Wada, E., and A. Hattori (1978), Nitrogen isotope effects in the assimilation of inorganic nitrogenous compounds by marine diatoms, *Geomicrobiology Journal*, *1*, 85-101
Wada, E. (1980), Nitrogen isotope fractionation and its significance in biogeochemical processes occurring in marine environments, *Isotope Marine Chemistry*, edited by E. Goldberg, Y. Horibe, K. Saruhashi, 375-398, Uchida Rokakuho, Toyko
Waser, N. A. D., P. J. Harrison, B. Nielson, S. E. Calvert, D.H. Turpin (1998), Nitrogen isotope fractionation during the uptake and assimilation of nitarte, nitrite, ammonium, and urea by a marine diatom, *Limno. and Oceanogr.*, *43*(2), 215-224
Wu, J., S. E. Calvert, C. S. Wong (1997), Nitrogen isotope variations in the northeast subarctic Pacific: Relationships to nitrate utilization and trophic structure, *Deep Sea Res. I*, *44*, 287-314

Wu, J., W. Sunda, E. A. Boyle, and D. M. Karl (2000), Phosphate depletion in the Western North Atlantic Ocean, *Science*, *289*, 759-762

Yoshikawa, C., Y. Yamanaka, T. Nakatsuka (2006), Nitrate-Nitrogen Isotopic Patterns in Surface Waters of the Western and Central Equatorial Pacific, *J. Oceanogr., 62*, 511-525

Zickfeld, K., M. Eby, and A.J. Weaver (2008), Carbon-cycle feedbacks of changes in the Atlantic meridional overturning circulation under future atmospheric CO2, *Global Biogeochem. Cycles, 22*(3), GB3024, doi 10.1029/2007GB003118

Process	*Symbol*	*Model Enrichment Factor (‰)*	*Field Estimates (‰)* [a]
Algal NO_3 Assimilation	ε_{ASSIM}	5	4 – 15
N_2 Fixation	ε_{NFIX}	1.5	0 – 2
Excretion	ε_{EXCR}	6	3 – 6
Water Column Denitrification	ε_{WCD}	25	22 – 30
Sedimentary Denitrification	ε_{SD}	0	0 – 4

[a] see Appendix A for references

Table 1: Nitrogen Isotope Model Enrichment Factors

Model	*r*	*RMS*
Control	0.68	0.84
Algal NO_3 Assimilation	0.59	0.90
N_2 Fixation	0.64	1.3
Excretion	0.67	0.89
Water Column Denitrification	0.29	0.97
Sedimentary Denitrification	0.65	0.90

Table 2: Global measures of $\delta^{15}NO_3^-$ model performance: correlation coefficient (*r*) and root mean squared (*RMS*) error normalized by the standard deviation of the observations.

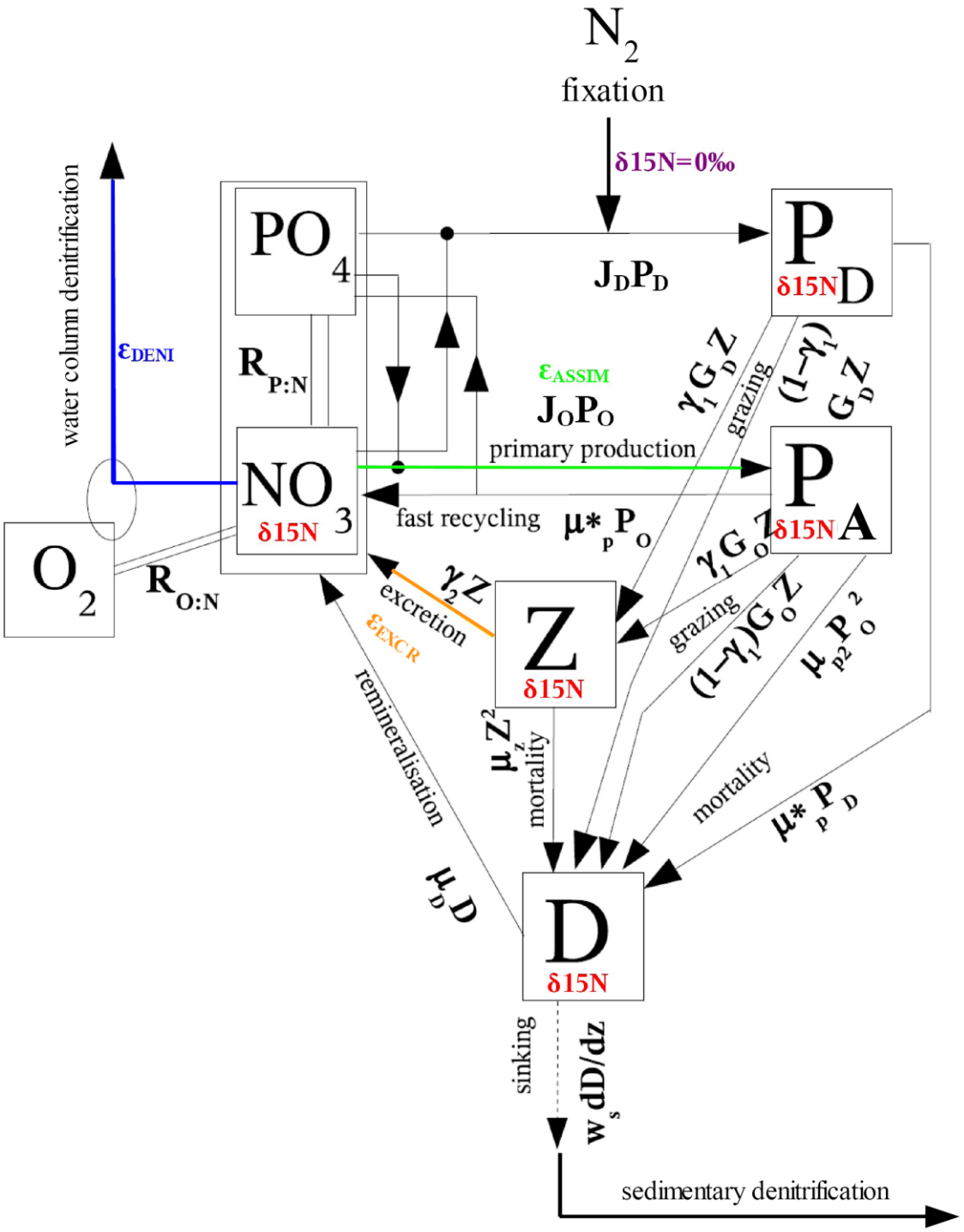

Figure 1. Schematic of the marine ecosystem model with the nitrogen isotope model parameters in color.

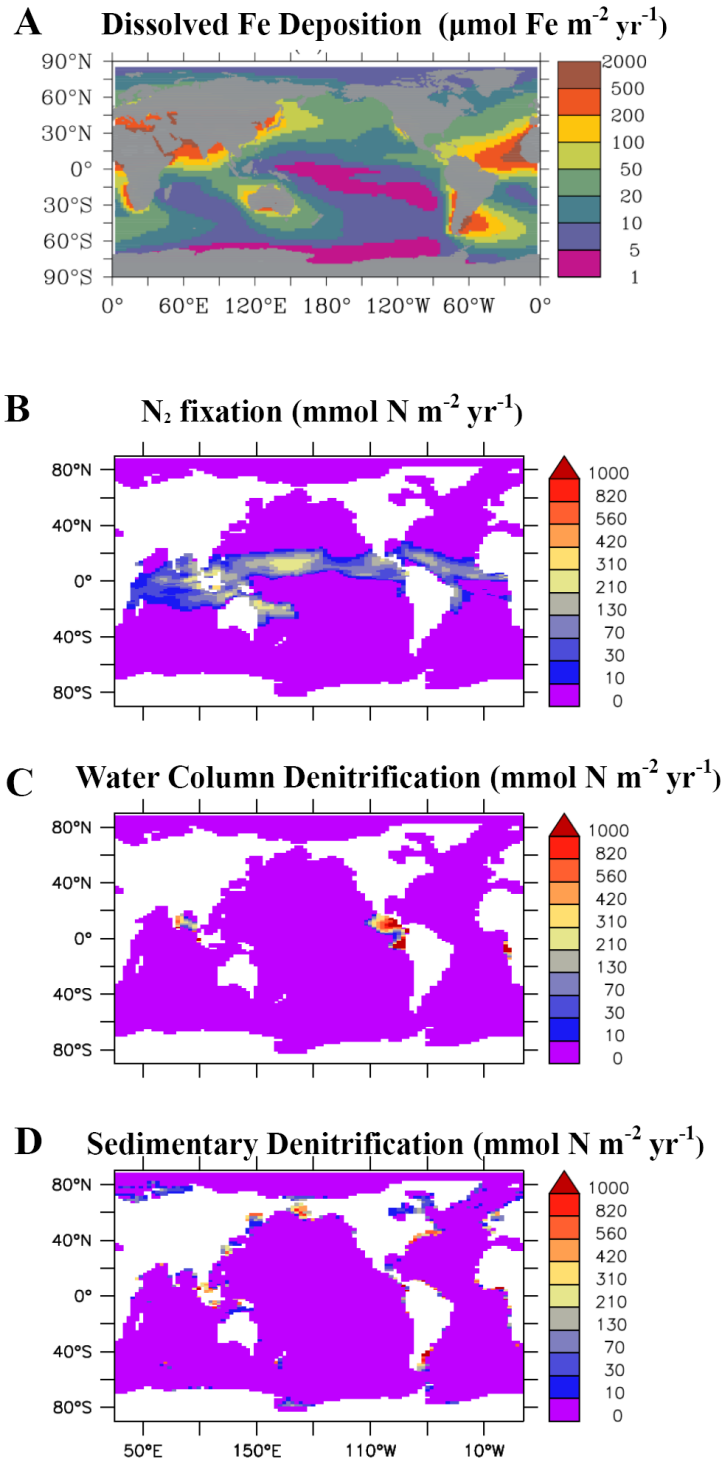

Figure 2. Estimated rate of annual (A) aeolian dissovled Fe deposition [*Fan et al.*, 2006] which limits (B) N_2 fixation when below ~10 µmol m^{-2} yr^{-1} (see text). Annual vertically integrated rates of (B) N_2 Fixation, (C) water column denitrification, and (C) sedimentary denitrification. Contour intervals are 210 and 1000 mmol N m^{-2} yr^{-1}.

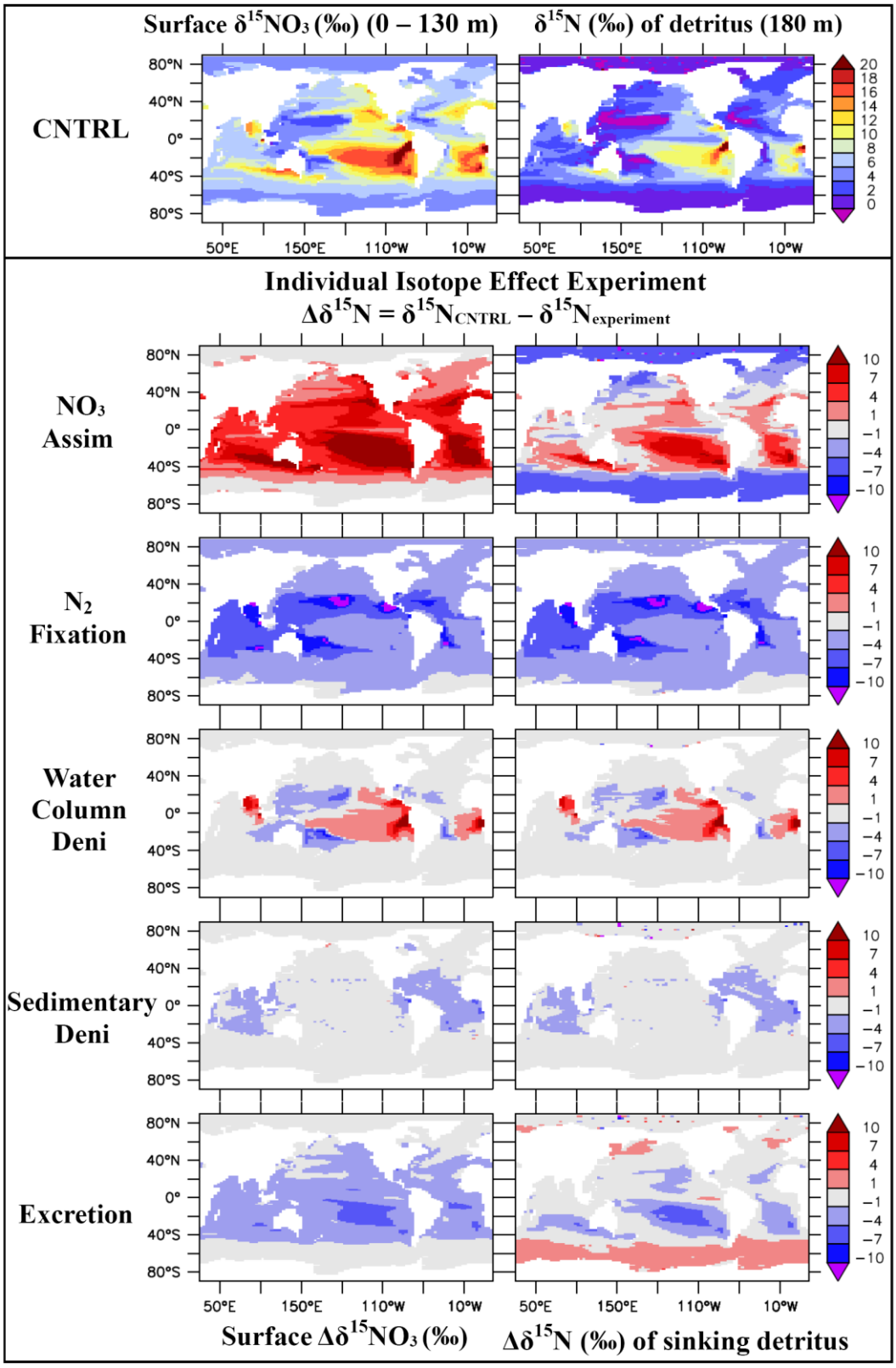

Figure 3. Top Panel: Surface $\delta^{15}NO_3$ and $\delta^{15}N$ of sinking detritus in the model. Bottom Panel: Isotope effect experiments where one isotope effect is neglected per simulation and its difference with CNTRL is shown to illustrate its individual effect on the CNTRL simulation.

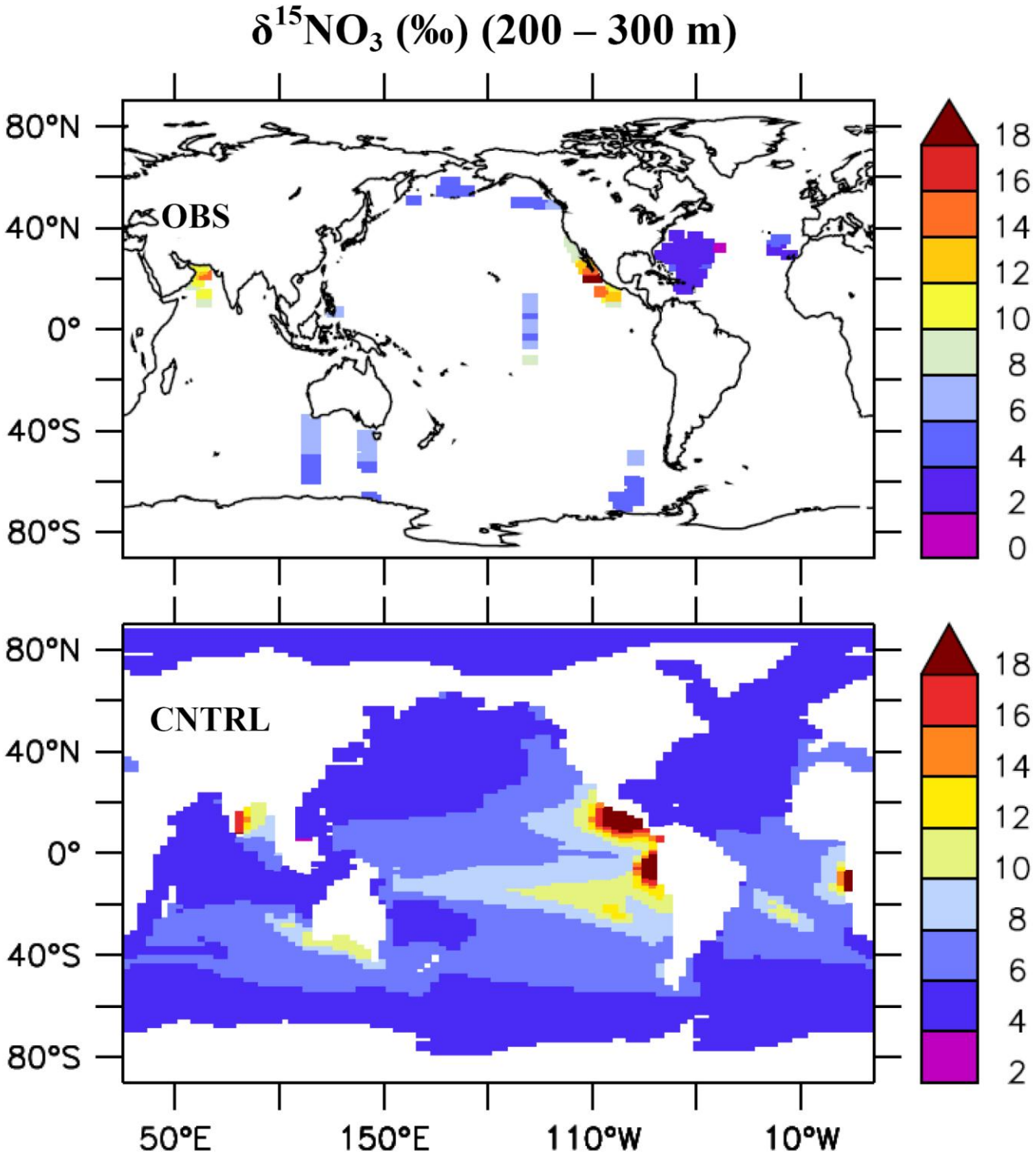

Figure 4. Comparison of annual $\delta^{15}NO_3$ (‰) averaged between 200 m - 300 m of available observations (OBS) and CNTRL. Due to the incomplete temporal coverage, seasonal biases in the annually averaged data exist depending on the region.

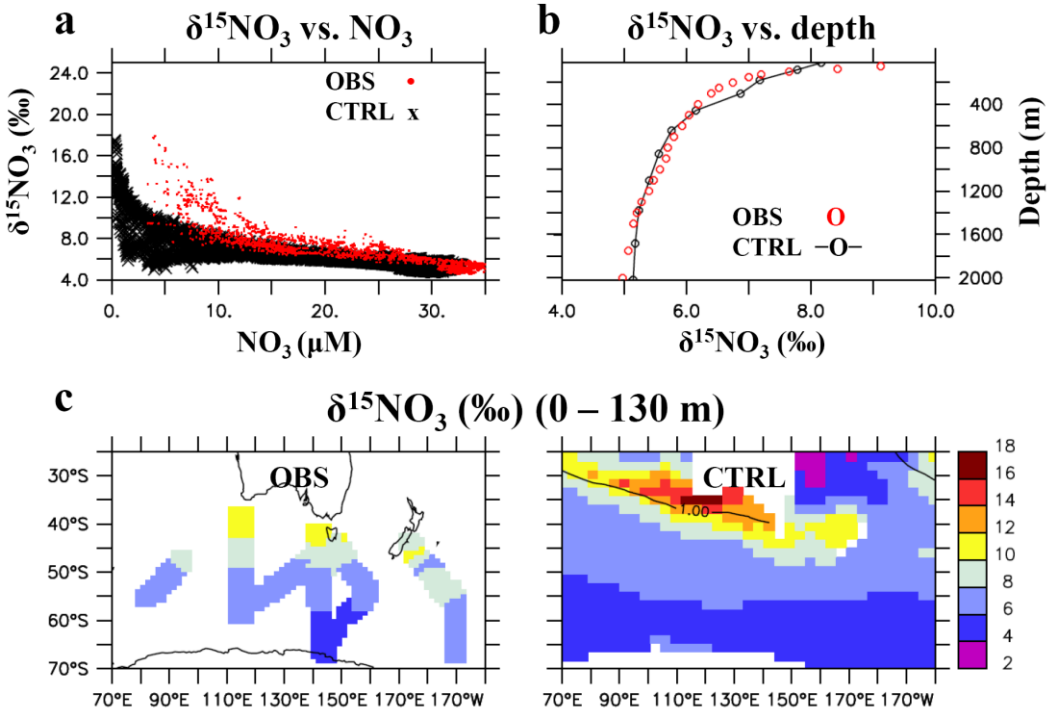

Figure 5. Comparison of the Indian-Pacific sector of the Southern Ocean with the $\delta^{15}NO_3$ database and CTRL. (a) $\delta^{15}NO_3$ vs. NO_3; (b) horizontally averaged (over available data) depth $\delta^{15}NO_3$ profiles; (c) surface $\delta^{15}NO_3$ and with a 1μM NO_3^- contour line.

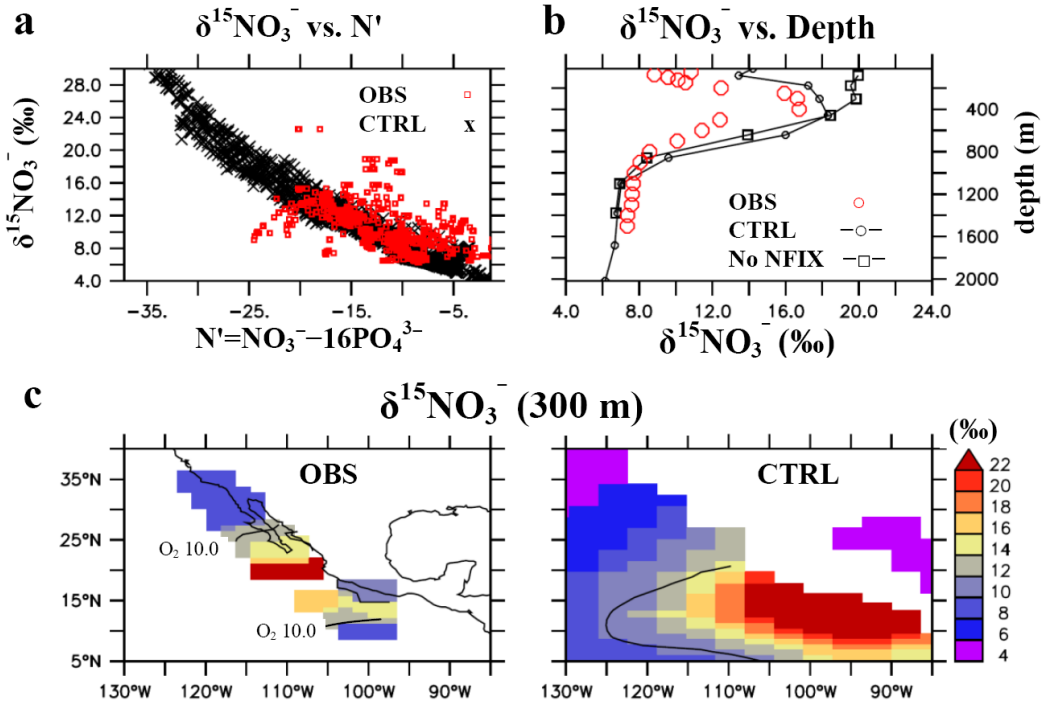

Figure 6. Comparison of the ETNP with the $\delta^{15}NO_3$ database and CTRL. (a) $\delta^{15}NO_3$ vs. N' = $NO_3^- - 16PO_4^{3-}$; (b) horizontally averaged (within 10 µM O_2 contour) depth $\delta^{15}NO_3$ profiles including the experiment where the isotope effect of N_2 Fixation is neglected (No NFIX); (c) subsurface $\delta^{15}NO_3$ with a 10 µM O_2 contour line.

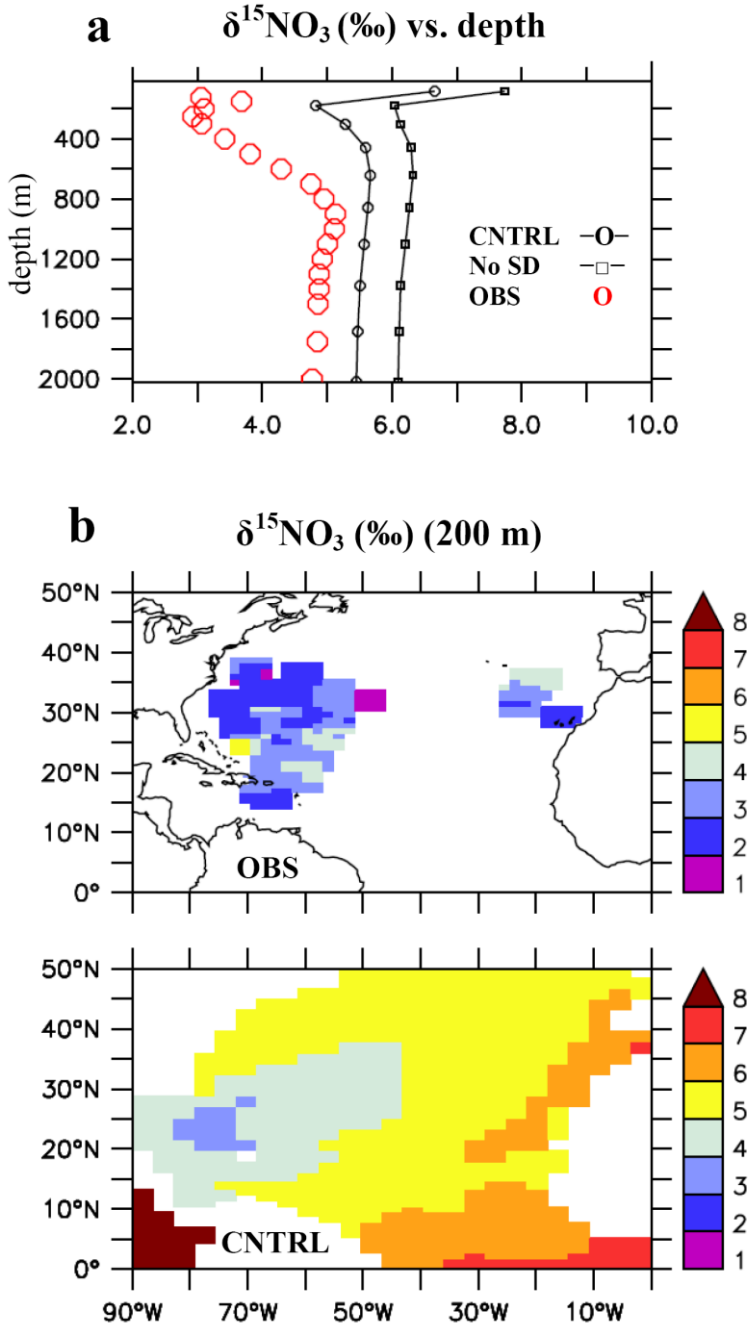

963
964

965 **Figure 7**. Comparison of the North Atlantic with the $\delta^{15}NO_3$ database and CNTRL. (a) horizontally
966 averaged (over available data) depth $\delta^{15}NO_3$ profiles including the experiment where sedimentary
967 denitrification is neglected (No SD); (b) subsurface $\delta^{15}NO_3$.